Copy 369
RM L55I13a

NACA RM L55I13a

NACA

RESEARCH MEMORANDUM

SOME EFFECTS OF SWEEP AND ASPECT RATIO ON THE TRANSONIC FLUTTER CHARACTERISTICS OF A SERIES OF THIN CANTILEVER WINGS HAVING A TAPER RATIO OF 0.6

By John R. Unangst and George W. Jones, Jr.

Langley Aeronautical Laboratory
Langley Field, Va.

NATIONAL ADVISORY COMMITTEE FOR AERONAUTICS

WASHINGTON

January 24, 1956

61

NATIONAL ADVISORY COMMITTEE FOR AERONAUTICS

RESEARCH MEMORANDUM

SOME EFFECTS OF SWEEP AND ASPECT RATIO ON THE TRANSONIC FLUTTER CHARACTERISTICS OF A SERIES OF THIN CANTILEVER WINGS HAVING A TAPER RATIO OF 0.6

By John R. Unangst and George W. Jones, Jr.

SUMMARY

An investigation of the flutter characteristics of a series of thin cantilever wings having taper ratios of 0.6 has been conducted in the Langley transonic blowdown tunnel at Mach numbers between 0.76 and 1.42. The angle of sweepback was varied from 0° to 60° on wings of aspect ratio 4, and the aspect ratio was varied from 2.4 to 6.4 on wings with 45° of sweepback. This investigation represents an extension and reanalysis of a similar investigation reported in NACA RM L53G10a. The previous data are presented again in this paper. More recently obtained data for some of the wings are also presented as well as data for an additional sweep angle of 30°.

The results are presented as ratios between the experimental flutter speeds and the reference flutter speeds calculated on the basis of incompressible two-dimensional flow. These ratios, designated the flutter-speed ratios, are given as functions of Mach number for the various wings. The flutter-speed ratios were characterized, in most cases, by values near 1.0 at subsonic speeds with large increases in the speed ratios in the range of supersonic speeds investigated. Increasing sweep effected increases in the flutter-speed ratios between 0° and 30° followed by progressive reductions of the speed ratios to nearly 1.0 as the sweep was increased from 30° to 60°. Reducing the aspect ratio from 6.4 to 2.4 resulted in progressively larger values of the flutter-speed ratios throughout the Mach number range investigated. The additional data obtained in this investigation substantially corroborate the trends established in NACA RM L53G10a.

INTRODUCTION

Several flutter investigations have been undertaken in the Langley transonic blowdown tunnel in order to provide experimental data on wing flutter in the transonic speed range. The results of two of these investigations are reported in references 1 and 2.

The present investigation represents an extension and reanalysis of the investigation of reference 2. Since the curves showing the variation of flutter-speed ratio (ratio of experimental to calculated flutter speed) with Mach number for some of the plan forms of reference 2 were defined by only a few points, more detailed data were obtained for these plan forms. An additional plan form of aspect ratio 4 with 30° of sweepback was tested. Both the new data and the data contained in reference 2 are presented herein. All of the experimental flutter records upon which the results presented in reference 2 were based have been reexamined to insure uniformity of definition of all flutter points, particularly those points where the exact start of flutter was somewhat obscure. As a consequence, some of the data presented in this paper differ in detail from those given in reference 2. As suggested in reference 2, additional modes were employed in the calculations of the reference flutter speeds for some of the wing plan forms.

The plan forms which were tested for this investigation consisted of wings of aspect ratio 4 with sweepback angles of 0°, 30°, 45°, and 60°. Data contained in reference 2 for these plan forms, for plan forms with 45° sweepback and aspect ratios of 2.4 and 6.4 (erroneously given as aspect ratios of 2 and 6 in reference 2), and for the plan form of aspect ratio 4 with $52\frac{1}{2}^\circ$ of sweepback are also presented in this paper. All the wings had a taper ratio of 0.6 and airfoil sections approximately 4 percent thick. The results are presented over a Mach number range from 0.76 to 1.42.

SYMBOLS

A — aspect ratio including body intercept, $\frac{(\text{Span})^2}{\text{Area}}$

a — distance perpendicular to quarter-chord line in wing semichords, from midchord to elastic axis position; positive rearward, $2x_o - 1$

A_g — geometric aspect ratio, $\frac{(\text{Exposed span})^2}{\text{Exposed area}}$

b — half-chord perpendicular to quarter-chord line, ft

b_r — half-chord perpendicular to quarter-chord line at intersection of quarter-chord line and wing root, ft

b_s half-chord measured streamwise at intersection of wing root and fuselage, ft

c wing chord perpendicular to quarter-chord line, ft

c_r wing root chord perpendicular to quarter-chord line, $2b_r$, ft

c_t wing tip chord perpendicular to quarter-chord line, ft

f_{h_i} measured coupled bending frequencies, cps ($i = 1, 2, 3$)

f_{b_i} uncoupled bending frequencies, cps ($i = 1, 2$)

f_t measured coupled torsion frequency, cps

f_α uncoupled first torsion natural frequency relative to elastic axis, $f_t\left[1 - \dfrac{\left(\dfrac{x_\alpha}{r_\alpha}\right)^2}{1 - \left(\dfrac{f_{h_1}}{f_t}\right)^2}\right]^{1/2}$ (except for 245 wing), cps

EI bending stiffness, lb-in.^{2}

GJ torsion stiffness, lb-in.^{2}

g structural damping coefficient

g_h structural damping coefficient in bending

g_α structural damping coefficient in torsion

I_α mass moment of inertia of wing section about elastic axis, slug-ft^2/ft

k reduced frequency, $b\omega/V$

l length of wing panels outside fuselage, measured along quarter-chord line, ft

M Mach number

m mass of wing per unit length along quarter-chord line, slugs/ft

q dynamic pressure, lb/sq in.

r_α nondimensional radius of gyration of wing section perpendicular to quarter-chord line about elastic axis, $\left(I_\alpha/mb^2\right)^{1/2}$

V stream velocity, fps

V_n component of stream velocity normal to quarter-chord line, fps

V_e/V_R flutter-speed ratio

x_o distance of elastic axis of wing section behind leading edge, percent chord

x_α distance perpendicular to quarter-chord line in semichords from wing elastic axis to wing-section center of gravity, positive for center of gravity behind elastic axis

η nondimensional coordinate along quarter-chord line, measured from intersection of quarter-chord line and fuselage, fraction of length l

μ mass ratio, at $\eta = 0.75$ station, $m/\pi\rho b^2$

λ taper ratio, $\frac{\text{Tip chord}}{\text{Chord in plane of symmetry}}$

Λ angle of sweepback of quarter-chord line, deg

ρ air density, slugs/cu ft

ω angular frequency of vibration, radians/sec

$\omega_{h_i},\omega_{b_i}$ angular bending frequency, radians/sec $\left(2\pi f_{h_i}, 2\pi f_{b_i}\right)$

ω_α angular uncoupled torsion frequency, radians/sec $\left(2\pi f_\alpha\right)$

θ semichord ratio, b/b_r, normal to quarter-chord line, $1 - \eta(1 - \text{Panel } \lambda)$

Subscripts:

e experimental values

R calculated values (corresponds to subscript Λ in ref. 4)

MODELS

Model Geometry

The models employed in the present investigation, together with the models of reference 2, represent a series of seven wing plan forms varying in sweep and aspect ratio. Five of the plan forms had aspect ratios of 4 and sweepback of the quarter-chord line of 0°, 30°, 45°, $52\frac{1}{2}^\circ$, and 60°. The other two plan forms were swept back 45° at the quarter-chord lines and had aspect ratios of 2.4 and 6.4. All wings had taper ratios of 0.6. All wings had NACA 65A004 streamwise airfoil sections, except the wing with aspect ratio 4 and sweepback of 60° which was approximately 5 percent thick. The ratio of sting diameter to wing span varied from 0.31 for the aspect-ratio-2.4 wings to 0.18 for the aspect-ratio-6.4 wings. Drawings of the various plan forms tested are presented in figure 1. Each of the plan forms is designated by a three-digit number; the first digit refers to the aspect ratio to the nearest integer and the last two digits refer to the angle of sweepback to the nearest degree. For example, the wing of aspect ratio 4 with 45° of sweepback is designated as the 445 wing.

Materials and Construction

The basic material used in the construction of the models tested in the present investigation, with one exception, was Compreg wood, a laminated, compressed, resin-impregnated maple. The 400 wing was made of solid Compreg. The 430 wing had a solid Compreg core wrapped with a 0.006-inch layer of Fiberglas. The construction of the 445 wing was changed from the solid Compreg used in reference 2 to a solid Compreg core wrapped with a 0.006-inch layer of Fiberglas. This was done in an attempt to assure the attainment of flutter in the tunnel over the desired Mach number range. All but one of the 460 wings had a solid Compreg core wrapped with a 0.018-inch layer of Fiberglas. One 460 wing was made of solid aluminum alloy and was perforated with a series of holes drilled through the wing to achieve the desired stiffness distribution. These holes were uniformly distributed over the wing plan form and were filled with rubber in order to obtain a continuous wing surface without appreciably altering the stiffnesses of the perforated wing (ref. 3).

The 245 wing of reference 2 had a tapered spar of pine 2 percent thick, with the grain direction parallel to the quarter-chord line. This spar was sandwiched between two layers of balsa 1 percent thick with the grain direction parallel to the airstream. The 452 wing of reference 2 had a solid Compreg core wrapped with a 0.006-inch layer of Fiberglas. The 645 wing of reference 2 was made of solid magnesium.

The wings which were wrapped with Fiberglas were made undersize prior to wrapping in order to obtain the desired thickness, but the streamwise airfoil sections of the 460 wings averaged a maximum thickness of 5 percent instead of the intended 4 percent after being covered with Fiberglas.

Physical Parameters

Elastic-axis location, section center-of-gravity location, structural damping coefficient in bending, spanwise distributions of mass and mass moments of inertia, and the frequencies corresponding to the first three, and in some cases four, natural modes of vibration were measured. The elastic-axis locations were obtained by determining, as nearly as possible, the chordwise position at which a concentrated bending load produced no twist in the wing. For the determination of the elastic-axis locations, each wing was clamped along a line perpendicular to the quarter-chord line and passing through the intersection of the wing trailing edge and the root. The mass, center-of-gravity locations, and mass moments of inertia (or radii of gyration) were obtained from strips of each wing cut perpendicular to the quarter-chord line. The structural damping coefficients were determined from the decrement of free bending vibrations in still air. Natural frequencies were determined from forced vibration tests of the wings rigidly mounted on a massive steel bench. A more detailed description of the methods of measurement of these parameters is given in reference 2.

Values of the geometric and physical properties of the models are found in table I. For each plan form only one representative set of physical parameters, with the exception of the natural frequencies, is presented for each type of model construction. Each plan form of reference 2 which is included in this paper is designated by reference 2 and representative values of the natural frequencies of the models of each plan form are given.

In addition to the above properties, measurements were made of the spanwise variation of the bending and torsional stiffnesses, EI and GJ, for some of the models. The method of measurement is described in reference 3. The results of the stiffness measurements are given in figures 2 to 7. In these figures, the symbols shown under Measurement indicate each attempt at measurement of that particular stiffness and thus the variations between symbols indicate the repeatability of the method.

APPARATUS AND TESTS

Wind Tunnel

The Langley transonic blowdown tunnel, which was used for these tests, is equipped with a slotted, octagonal test section which allows the tunnel to operate from subsonic speeds through and above sonic speed to a Mach number of about 1.45. A plan view of the tunnel, with a model installed, and a cross-sectional view of the test section are shown in figure 8.

A variable and continuous regulation of the air flow is allowed by a set of three plug valves, located between a high-pressure reservoir and the tunnel, which are operated by a single control. A quick-operating mechanism closes the valves in approximately 1/2 second.

The test-section Mach number is controlled by the valve opening, which governs the stagnation pressure, and by the size of the orifice plate installed downstream of the test section. When choked, an orifice permits a specific test-section Mach number to be maintained as the stagnation pressure, and hence air density, is varied from the value at which the orifice chokes to the maximum design pressure, 75 pounds per square inch. Since the occurrence of flutter depends on air density as well as velocity and Mach number, this technique, along with proper model design, permits flutter to be obtained throughout the Mach number range on the same model. Figure 9 shows the variation of dynamic pressure as a function of test-section Mach number for three orifice plates. A sufficient number of orifice plates are available to choke the tunnel over a Mach number range between 0.85 and 1.4 in Mach number increments of approximately 0.06. The tunnel may be choked at Mach numbers below 0.85 by attaching inserts to the 0.85 orifice. Mach numbers above approximately 1.4 are obtained by bleeding off part of the air in the tank surrounding the slotted test section. It should be noted that the test-section velocity is not uniquely defined by the Mach number because of the variation of tunnel stagnation temperature with initial reservoir conditions and expansion in the reservoir during each run. The tunnel is equipped with a viewing screen, not shown in figure 8, which allows observers to watch the model throughout the tunnel operation.

Support System

The wings were mounted at 0° angle of attack on a 3-inch-diameter cylindrical sting fuselage. A fixed wing root condition was obtained by mounting the wing with close-fitting filler blocks and four 3/8-inch bolts. Figure 10 shows a flutter model mounted on the sting fuselage. The fuselage nose extended into the subsonic flow region of the tunnel entrance cone in order to prevent the formation of a bow shock wave and its associated reflection from the tunnel walls onto the model. The support system was considered to form a rigid mount since the mass of the system was very large compared with the mass of a model. The measured fundamental bending frequency of the support system was approximately 15 cycles per second.

It will be noted in figure 10 that there was a small bump in the sting fuselage behind the model. The shock wave which formed near this bump at transonic speeds may, for a limited Mach number range, have crossed the outer portions of the more highly swept wings, notably the 460 wings. The absence of any consistent irregularities in the experimental data, however, suggests that the presence of this shock wave had a negligible effect on the results.

Instrumentation

Each model was instrumented with strain gages externally mounted on the wing near the root and oriented so as to distinguish between wing bending and torsion deflections. However, the gages could not be oriented so as to eliminate completely cross coupling between the bending and torsion signals. The strain gages were used to provide an indication of the start of flutter and to obtain a record of the frequency of wing bending and torsion oscillations.

During the tests, a multichannel recording oscillograph was used to make simultaneous recordings of the strain-gage signals, tunnel stagnation pressure and temperature, and test-section static pressure. A sample test record is given in figure 11 in which the start of flutter is shown by the change in the wing oscillations from an irregular form to a near sine wave, the amplitude of which rapidly increased. During the more recent tests, the strain-gage signals of each wing were fed into a cathode-ray oscilloscope, the bending signals to the vertical axis, and the torsion signals to the horizontal axis. A simple closed geometric pattern resulted at flutter, and thus aided the model observer in determining the start of flutter.

A high-speed, 16-mm motion-picture camera (approximately 1,000 frames per second) was used to obtain a visual record of wing deflection during some of the flutter tests. These films served as an aid in defining the mode shape and magnitude of flutter.

Tests

The objectives of the wind-tunnel test program were to determine the flutter characteristics of each wing at 0° angle of attack for several transonic Mach numbers. The procedure followed in obtaining model flutter at a particular Mach number was to increase the stagnation pressure gradually until flutter was seen by an observer viewing the model. The stagnation pressure and, consequently, Mach number, were then held constant for a brief interval at initial flutter conditions, after which the air flow was quickly stopped in an effort to save the model from destruction. Small adjustments in angle of attack were made when necessary in order to trim the models to the zero-lift condition.

METHODS OF ANALYSIS

General Considerations

A true indication of the effects of plan-form variation on the flutter speed in the transonic Mach number range cannot be obtained from a simple comparison of experimental flutter speeds. Because of the operating characteristics of the tunnel, the density, and hence mass ratio μ, varied for the different Mach numbers at which flutter was obtained. Furthermore, the torsional frequency ω_α as well as the nondimensional parameters x_α, a, r_α, and ω_h/ω_α varied for the different plan forms and, in some cases, for the different models of the same plan form. Therefore, in an effort to separate the effects of plan-form and Mach number variation from the effects of these other variables, the results are presented in the form of a ratio of experimental flutter speed to calculated, or reference, flutter speed V_e/V_R as a function of Mach number (as set forth in ref. 4) for the various plan forms tested.

Reference Flutter Speed

The method of calculating the reference flutter speeds is the same as that employed in reference 2 which was based on the type of analysis of reference 4. Briefly, the procedure as applied in this paper employs two-dimensional incompressible aerodynamic coefficients in a Rayleigh-type analysis in which the flutter mode is approximated by the superposition of uncoupled, free vibration modes of a uniform cantilever beam. The aerodynamic coefficients are based on the component of the free-stream velocity normal to the quarter-chord line. The spanwise derivative of the velocity potential, appearing in the method of reference 4, has been neglected.

The effective wing root and tip are defined in the present analysis as the perpendiculars to the quarter-chord line at the intersections of the quarter-chord line with the actual root and tip, respectively.

The values of k were weighted along the span in accordance with the wing taper, and the spanwise variation of the Theodorsen functions F(k) and G(k) were approximated by a straight line between the root and tip values. The solution of the flutter stability determinant was obtained in the form of the structural damping coefficient g as a function of $V_n/b_r\omega_\alpha$. The structural damping coefficient used was that measured in bending with the assumption that $g_h = g_\alpha = g$.

The V_R calculations of reference 2 were based on a flutter mode approximated by the uncoupled first bending and first torsion modes of a uniform cantilever beam. These calculations resulted in flutter speed ratios which were considerably below 1.0 in the subsonic and low supersonic speed range for wings with relatively high l/c_r ratios. Examination of motion pictures showing the mode shape at flutter, and the proximity of ω_{h_2} to ω_α for some of the wings, suggested that the inclusion of higher modes in the calculations might result in better agreement between experimental and calculated flutter speeds at subsonic Mach numbers. Calculations of V_R were accordingly made using the uncoupled first and second bending and first torsion uniform cantilever modes for the 445, 452, 460, and 645 plan forms. In addition, a four-mode analysis was made for a few of the points for the 460 wing, the fourth mode being the third uncoupled bending mode. Only the first bending and torsion modes were used in the calculations for the other wings.

The measured frequencies of the predominantly bending modes were taken to be the uncoupled values, except for the 245 wing, whereas the measured frequencies of the predominantly torsion modes were adjusted to the uncoupled values. For all the wings except the 245, the uncoupled torsion frequency was inferred from the coupled values by the simplified formula given in reference 4 and in the Symbols section herein. Since the vibration modes of the 245 wing were highly coupled, the uncoupled torsion and bending frequencies were determined from the measured coupled values for this wing by means of a Rayleigh-type analysis in which the first three coupled wing modes were expressed in terms of the uncoupled first and second bending and first torsion modes of a uniform cantilever beam. A number of calculations indicated that, in comparison with the more elaborate method employed for the 245 wing, the simplified uncoupling formula of reference 4 was entirely adequate for the other wings.

RESULTS

General Comments

Visual observations, examination of high-speed motion-picture films and oscillograph records, and comparison of flutter frequencies with natural frequencies indicated that the flutter obtained in the tests was of the classical bending-torsion type. The wing oscillations at flutter, however, did not necessarily show a continual increase in amplitude with increasing time, but rather reached a constant amplitude. It was also noted that the flutter characteristics of the wings at subsonic speeds differed from those at supersonic speeds. Flutter at high subsonic Mach numbers, near 0.85, occurred with a relatively large amplitude and low frequency, whereas at supersonic Mach numbers, near 1.3, the flutter occurred with a lower amplitude and a higher frequency.

The beginning of flutter was not always as easily defined as that shown in figure 11, particularly at supersonic speeds. In many cases, the oscillograph records revealed a period of intermittent sinusoidal oscillations in both bending and torsion followed by a period of steady continuous flutter as the tunnel conditions approached and crossed the flutter boundary. A sample oscillograph record of one of the test runs showing this kind of behavior is shown in figure 12. For this particular test run, the beginning of a period of intermittent sinusoidal oscillations in bending and torsion might be chosen near point C for both wing panels. At point D, the oscillations of the right wing become nearly sustained and the frequencies in bending and torsion appear identical so that point D is defined as a flutter point. The oscillations of the left wing, however, remain intermittent in character until point E is reached. For cases such as that illustrated in figure 12, a clear-cut distinction between the period of intermittent oscillations and the start of flutter was difficult to make.

For those cases in which flutter did not exhibit a clearly defined start, time-history studies of the frequencies present in the bending and torsion oscillations were made to assist in defining the flutter point. These studies consisted of envelopes of the frequency spectra in bending and torsion plotted against tunnel dynamic pressure. As an example, a frequency study was made for the test record shown in figure 12 and is presented in figure 13. The frequency values at each labeled point in figure 12 were determined by counting the oscillations over a short period of time (about 0.01 second) at several values of time before and after the chosen point and are indicated in figure 13 by corresponding letters. Any one frequency which seemed to predominate among the various values obtained is shown as the predominant frequency in figure 13, and the highest and lowest frequencies obtained are shown as the boundaries of the frequency envelope. Since the oscillations were counted over a short-time interval, there is some degree of judgment involved and the frequency values shown should be considered as only approximate. The points where the predominant bending and torsion frequencies first become equal, as shown by points E and D on figures 13(a) and (b), respectively, are defined as flutter points. The points of initial overlapping of the boundaries of the frequency spectra in bending and torsion (point C in figs. 12 and 13) are arbitrarily defined as the beginning of periods of intermittent sinusoidal oscillations which in this paper are called low-damping regions. These periods should be interpreted as regions of uncertainty in which the wing may or may not have been fluttering. Some indication of the beginnings of the low-damping regions in relation to the points of flutter is given in the later figures of this paper. It should be noted that the amplitude of the intermittent oscillations experienced by the models preceding flutter is dependent upon the aerodynamic and structural damping of the models and upon the magnitude and frequency of the exciting disturbances experienced by the models. Since tunnel turbulence, no doubt, provides most of the excitation experienced by the models, the magnitude of the intermittent oscillations observed on the models preceding flutter is probably not representative of what would be obtained in free air.

In many cases, the two panels of the same model did not flutter simultaneously. This was quite probably due to differences in physical properties, notably the natural frequencies, between wing panels. In those cases, separate flutter points are presented for the start of flutter for each panel. It was also noted that more than one flutter point frequently occurred during a single run. The reason for this behavior is illustrated in figure 9 which shows that for a given tunnel-orifice condition (in this case, the $M = 1.25$ orifice was installed), the tunnel-operating curve can intersect the flutter boundary curve of a wing at more than one point. For the example of figure 9, three flutter points would be obtained during the run (points A, B, and C). In such cases, each of the points is presented in the data.

Presentation of Results

The results of the investigation are presented in table II and are plotted in figure 14. Table II contains the results of theoretical calculations and experiments with some indication of the different models employed, the behavior of each wing panel during a particular test run, and values of the pertinent flutter parameters. Column 1 gives the identification numbers of the models employed in obtaining the data. A model designation of reference 2 in column 1 indicates that the data are taken from reference 2 in which no record was kept of the numbers of individual models of the same plan form and construction. Columns 2 and 3, respectively, show the run number and the chronology of the data points during a particular run. (A single run is defined as one operation of the tunnel, starting with the opening of the valves and ending with the closing of the valves.) For example, for a given run in column 2, a designation of 1, 2, 3, . . . in column 3 refers to the first, second, third, . . . data point obtained during that run. Columns 4 and 5 contain a code system describing the behavior of each wing panel at each data point. The following designations are used to describe the data points:

N no flutter

F flutter

D low damping

G strain gages inoperative

E end of flutter with dynamic pressure increasing

X wing panel destroyed or not installed

Subscripts 1 or 2 attached to these designations refer to the first or second occurrence of flutter on the panel during a particular run. For example, a series of data points obtained during a given run might be coded as follows:

Run	Point	Left	Right
3	1	F_1	F_1
	2	E_1	E_1
	3	D_2	D_2
	4	F_2	D_2
	5	F_2	F_2

Then, from this example, it will be seen that during this run: at point 1, both panels started to flutter for the first time; at point 2, both panels stopped fluttering; at point 3, both panels exhibited behavior which has been previously defined as low damping; at point 4, the left panel fluttered a second time during the run but the right panel continued low-damping behavior; and at point 5, the right panel fluttered a second time while the left panel continued to flutter.

Presented in figure 14 are the results of the investigation in the form of plots of the ratio of experimental to calculated flutter speed V_e/V_R as a function of Mach number for the various plan forms tested. The low-damping regions are indicated on these plots by dotted lines extending from the beginning of the low-damping period to the point of definite flutter. The direction of these dotted lines is indicative of the manner in which the speed and Mach number varied as the flutter condition was approached during the tunnel tests. The points indicating flutter are shown on the plots by means of plain symbols. The points showing the end of a flutter period are indicated on the plots by means of shaded symbols.

The following paragraphs contain some general comments concerning the data presented in figure 14 for each of the plan forms and, in a few cases, some observations regarding the behavior of the wings during the tests. It should be noted that all the data presented in reference 2 were reexamined for presentation in this paper; hence, some of the data may differ in detail from those previously presented.

245 plan form.- The data presented herein for the 245 wings (fig. 14(a) and table II(a)) are taken entirely from reference 2. It should be noted the aspect ratio of this plan form is 2.4 instead of 2 as previously reported. Low-damping periods could not be determined with any degree of certainty, because it was impossible to distinguish separate bending and torsion frequencies on the flutter records. This difficulty was due to the poor orientation of the strain gages on this wing, resulting in flutter records which showed only bending oscillations. Consequently, the data points presented represent only definite flutter points, but they do not necessarily identify the precise flutter boundary for this wing because of the difficulty in determining the exact start of flutter. All calculations of the reference flutter speeds were made with a two-mode analysis.

400 plan form.- The data presented herein for the 400 wings (fig. 14(b) and table II(b)) include the results presented in reference 2 and the results of more recent tests. Considerable difficulty was encountered in obtaining flutter on these wings because of a tendency toward static divergence. During the attempts to obtain flutter, several of these models diverged to destruction before fluttering. All calculations of the reference flutter speeds were made with a two-mode analysis.

430 plan form.- All the data presented for the 430 wings in figure 14(c) and table II(c) were obtained during this investigation. The data were obtained on five models, the physical parameters of which are given in table I(c). All calculations of the reference flutter speeds were made using a two-mode analysis.

445 plan form.- The data presented for the 445 wings in figure 14(d) and table II(d) include the data published in reference 2 and data obtained from the present investigation. The new data were obtained on two models, the physical parameters of which are given in table I(d). These new data were obtained in order to provide a clarification of the effect of Mach number on the flutter-speed ratio in the supersonic speed range. All the calculations of the reference flutter speeds presented in figure 14(d) and table II(d) were made using a three-mode analysis.

452 plan form.- All the data for the 452 wings presented in figure 14(e) and table II(e) were published previously in reference 2. In addition to reexamination of these data, the calculations of the reference flutter speeds were revised using a three-mode analysis.

460 plan form.- The data presented for the 460 wings in figure 14(f) and table II(f) include the data published in reference 2 and data obtained during this investigation. The new data were obtained in order to clarify the location of the flutter boundary in the subsonic speed range. The flutter obtained on this plan form in the subsonic speed range was very violent and frequently caused the Compreg-wood wings to crack within the fuselage block near the root. Ignorance of the existence of such a condition may explain the two points at $M \approx 0.83$ which are below the curve in figure 14(f). The calculations of the reference flutter speeds were made using a three-mode analysis.

645 plan form.- All of the data presented for the 645 wings in figure 14(g) and table II(g) were published previously in reference 2. It should be noted that the aspect ratio of this plan form is 6.4 instead of 6 as previously reported. In addition to reexamination of these data, the calculations of the reference flutter speeds were revised using a three-mode analysis.

DISCUSSION

Effects of Sweep on the Flutter-Speed Ratio

The effects of sweepback angle on the variation of the flutter-speed ratio with Mach number are shown in figure 15 for wings with aspect ratio of 4 and sweepback of 0°, 30°, 45°, $52\frac{1}{2}^{\circ}$, and 60°. This figure shows the faired curves of figure 14 for the appropriate plan forms. Examination of figure 15 shows that the results obtained from this investigation are similar to those given in reference 2 in that V_e/V_R is near 1.0 for subsonic Mach numbers, V_e/V_R increases with Mach number for supersonic Mach numbers, and the effect of Mach number on V_e/V_R is considerably reduced for wings with large sweepback. Figure 15 shows that the flutter-speed ratio increases as the sweepback angle is increased from 0° to 30°; further increases in the sweepback angle from 30° to 60° are shown to result in a progressive reduction in the flutter-speed ratio to values which are near 1.0 throughout the Mach number range for the 60° sweptback plan form. Contrary to the results reported in reference 2, the data for the unswept wings are seen to fall below the curve of V_e/V_R plotted against Mach number for the 45° swept wings at supersonic speeds. The difference in the trends shown herein as compared to those of reference 2 results from the more complete data presently available for the 45° swept wings and not from any basic change in the data for the unswept wings. On the other hand, difficulty was experienced in obtaining flutter on some of the models of the unswept wing because of a strong tendency toward static divergence. The probability therefore exists that the flutter boundary of the wing may have been affected by the divergent tendencies. In any case, there appears to be a need for further study of low-aspect-ratio unswept wings and the effect of variations in sweep angle between 0° and 30°.

Effects of Aspect Ratio on the Flutter-Speed Ratio

The effects of aspect ratio on the variation of the flutter-speed ratio with Mach number are shown in figure 16 for wings with sweepback of 45° and aspect ratios of 2.4, 4, and 6.4. This figure shows the faired curves of figure 14 for the appropriate plan forms.

Figure 16 shows a large increase in flutter-speed ratio at the higher supersonic Mach numbers investigated as the aspect ratio is reduced from 6.4 to 4. It will be noted that a similar large increase in flutter-speed ratio is shown in the subsonic region as the aspect ratio is reduced from 4 to 2.4. This fairly large increase in flutter-speed ratio which accompanies a reduction in aspect ratio from 4 to 2.4 is probably due, at least in part, to inadequacies in the aerodynamic coefficients employed in the reference flutter-speed calculations, although other uncertainties arise in the attempt to treat the 245 wing as a simple beam.

Effects of Additional Modes on the Reference Flutter Speed

The results presented in reference 2 showed that for certain of the plan forms the values of the reference flutter speeds obtained using two modes in the calculations tended to be too high, thus yielding poor agreement between calculated and experimental flutter speeds. Consequently, in the present paper calculations of the reference flutter speeds were made using three modes for the 445, 452, 460, and 645 plan forms in an attempt to improve the agreement between V_e and V_R. A comparison of the flutter-speed ratios calculated with two modes and with three modes is shown in figures 17 to 20. In all cases, the addition of a third mode, the second uncoupled bending mode, is seen to result in reduced values of the reference flutter speeds and corresponding improvements in the agreement between V_e and V_R at subsonic Mach numbers. It will be noted from figures 17 to 20 and table I that the effect of the addition of a third mode is related to the ratio of second bending to first torsion frequency. Within the range of the wings considered herein, the lower the second bending frequency with respect to the first torsion frequency, the greater is the effect of the addition of a third mode. The addition of a third mode is seen to have relatively little effect in the case of the 445 wing. Since the ratios of second bending to first torsion frequencies of the 400, 430, and 245 wings were even higher than was the case for the 445 wing, only two modes were used in the analysis of these wings. The addition of a fourth mode, the third uncoupled bending mode, to the calculations for the 460 wing is seen in figure 19 to have little or no effect on the reference flutter speed.

Application of the Flutter-Speed Ratio

As pointed out in reference 2, caution should be exercised in applying the flutter-speed ratios to the determination of the flutter speed of wings which have values of ω_h/ω_α, x_α, a, r_α, and μ much different from those which characterize the wings of the present investigation. It might be hoped that the reference flutter-speed calculations, as obtained in the present paper, have adequately removed from the results the effects of such variables as the center-of-gravity position, and that the curves of V_e/V_R against Mach number are a function of plan form only. It is not entirely evident, however, that such is the case and it is thought that further investigation of particular wing plan forms having different values of the various pertinent parameters which are used in the reference speed calculation are required in order to establish the applicability of the results obtained.

Modified Experimental Flutter-Speed Coefficient

In order to provide some physical idea of the relationship between wing torsional frequency, flutter speed, and flutter mass-density ratio, figure 21 has been prepared. In this figure, faired curves of an experimental flutter-speed coefficient corrected for mass-density ratio $V_e/b_s\omega_\alpha\sqrt{\mu_e}$ are shown as a function of Mach number for all the plan forms tested. The values of the experimental flutter-speed coefficient, its components, and the values of Mach number used to obtain the data points through which the faired curves of the figure are drawn were taken from tables I and II. It should be noted that curves of the parameter $V_e/b_s\omega_\alpha\sqrt{\mu_e}$ against Mach number implicitly contain the effects of such important parameters as radius of gyration, center-of-gravity position, and frequency ratio. The data of figure 21 indicate, except for the 245 wing, a spread of about 30 percent in the parameter $V_e/b_s\omega_\alpha\sqrt{\mu_e}$ at subsonic speeds with the 400 wing having the highest and the 460 wing the lowest values. For a given mass ratio, wing chord, and torsional frequency, the flutter-speed coefficients for the 245 wing are in the order of twice as great as that of any of the other wings. In general, the variation of $V_e/b_s\omega_\alpha\sqrt{\mu_e}$ with Mach number seems to be about the same as the variation of flutter-speed ratio V_e/V_R with Mach number. (See figs. 15 and 16.)

An interesting application of figure 21 may be seen if, for a given plan form, the coefficient $V_e/b_s\omega_\alpha\sqrt{\mu_e}$ is evaluated and plotted against

Mach number for values of V_e, μ_e, and M_e corresponding to flight conditions rather than flutter conditions. Some results of such an application are shown in figure 22, in which two example flight paths are shown in relation to the flutter boundary for the 445 plan form. The straight-line flight path indicates the relation between velocity and Mach number for constant altitude operation, with the slope of the line being given by $a/b_s\omega_\alpha\sqrt{\mu_e}$. (The speed of sound corresponding to the given altitude is given by a.) The flight path indicated by the curved dashed line corresponds to a high-speed dive. Any intersections of these flight paths with the flutter boundary of the plan form considered indicate a flutter condition. It should be noted that, for constant altitude operation of a plan form whose flutter boundary is characterized by a "knee," as at A in figure 22, the minimum altitude at which the wing will be flutter free throughout the Mach number range for which data are given is the altitude corresponding to the straight-line flight path which just misses the knee of the flutter boundary. For wings such as the 460, however, no knee exists in the flutter boundary shown in figure 21, at least within the scope of the data presented. Therefore, any constant altitude path plotted for the 460 plan form on figure 21 will intersect the 460 flutter boundary at some Mach number. If, for any of the plan forms shown in figure 21, a high-speed dive is executed, an intersection with the flutter boundary may occur at the highest Mach numbers for which data are given, even for wings whose flutter boundaries are characterized by knees in the transonic range.

CONCLUSIONS

The results of an investigation of some of the effects of wing sweep and aspect ratio on the flutter characteristics of a series of thin cantilever wings at transonic speeds indicated the following conclusions:

1. The variation of flutter-speed ratio with Mach number was characterized, in most cases, by flutter-speed ratios near 1.0 at Mach numbers near 0.8, and an increase in flutter-speed ratio in the supersonic region up to Mach numbers near 1.4.

2. The rate of increase of the flutter-speed ratio with Mach number in the supersonic region increased as the sweep angle was increased from 0° to 30°, and then progressively decreased as the sweep angle was increased from 30° to 60°.

3. Reducing the aspect ratio from 6.4 to 2.4 resulted in progressively larger values of the flutter-speed ratio throughout the Mach number range of this investigation.

4. The use of the second uncoupled bending mode in addition to the uncoupled first bending and torsion modes in the reference flutter-speed calculations resulted, in many cases, in better agreement between the calculated and experimental flutter speeds at subsonic Mach numbers.

Langley Aeronautical Laboratory,
National Advisory Committee for Aeronautics,
Langley Field, Va., September 9, 1955.

REFERENCES

1. Bursnall, William J.: Initial Flutter Tests in the Langley Transonic Blowdown Tunnel and Comparison With Free-Flight Flutter Results. NACA RM L52K14, 1953.

2. Jones, George W., Jr., and DuBose, Hugh C.: Investigation of Wing Flutter at Transonic Speeds for Six Systematically Varied Wing Plan Forms. NACA RM L53G10a, 1953.

3. Land, Norman S., and Abbott, Frank T., Jr.: A Method of Controlling Stiffness Properties of a Solid-Construction Model Wing. NACA TN 3423, 1955.

4. Barmby, J. G., Cunningham, H. J., and Garrick, I. E.: Study of Effects of Sweep on the Flutter of Cantilever Wings. NACA Rep. 1014, 1951. (Supersedes NACA TN 2121.)

TABLE I.- PHYSICAL PROPERTIES OF MODELS

(a) 245 Plan Form

Parameter	Model of Ref. 2
NACA section	65A004
A	2.4
Λ, deg	45
λ	0.6
Panel λ	0.685
Span, ft	0.808
A_g	0.91
l, ft	0.306
b_r, ft	0.129
b_s, ft	0.183
g_h	0.023

η	Model of Ref. 2				
	x_α	a	r_α^2	m	θ
0.05	-0.64	0.53	0.66	0.00217	0.98425
.15	-.66	.55	.69	.00207	.95275
.25	-.68	.57	.72	.00198	.92125
.35	-.70	.59	.74	.00189	.88975
.45	-.72	.61	.77	.00179	.85825
.55	-.74	.63	.80	.00170	.82675
.65	-.76	.65	.83	.00161	.79525
.75	-.78	.67	.86	.00152	.76375
.85	-.80	.69	.89	.00143	.73225
.95	-.82	.71	.92	.00134	.70175

Frequency	Model of Ref. 2
	Left and right
f_{h_1}	135
f_{h_2}	630
f_{t_1}	425
f_{b_1}	149
f_{b_2}	519
f_{α_1}	265
$(\omega_{b_1}/\omega_{\alpha_1})^2$	0.3161
$(\omega_{b_2}/\omega_{\alpha_1})^2$	3.836

TABLE I.- Continued

(b) 400 Plan Form

Parameter	Model no. 1 and Model of Ref. 2
NACA section	65A004
A	4
Λ, deg	0
λ	0.6
Panel λ	0.657
Span, ft	1.142
A_g	1.65
l, ft	0.445
b_r, ft	0.163
b_s, ft	0.163
g_h	0.02

η	Model of Ref. 2; Model no. 1				
	x_α	a	r_α^2	m	θ
0.05	0.14	-0.23	0.24	0.00738	0.98285
.15	.12	-.22	.25	.00716	.94855
.25	.11	-.21	.26	.00671	.91425
.35	.09	-.19	.27	.00617	.87995
.45	.08	-.18	.28	.00563	.84565
.55	.06	-.16	.28	.00509	.81135
.65	.05	-.15	.28	.00455	.77705
.75	.03	-.13	.27	.00400	.74275
.85	.02	-.11	.25	.00345	.70845
.95	.004	-.10	.24	.00291	.67415

Frequency	Model of Ref. 2	Model no. 1	
	Left and right	Left	Right
f_{h_1}	147	147	154
f_{h_2}	630	680	725
f_{t_1}	407	390	404
f_{α_1}	402	385	399
$(\omega_{h_1}/\omega_{\alpha_1})^2$	0.133	0.146	0.149
$(\omega_{h_2}/\omega_{\alpha_1})^2$	2.456	3.120	3.295

TABLF I.- Continued

(c) 430 Plan Form

Parameter	Models 1, 2, 3, 4, and 5
NACA section	65A004
A	4
Λ, deg	30
λ	0.6
Panel λ	0.657
Span, ft	1.142
A_g	1.65
l, ft	0.515
b_r, ft	0.149
b_s, ft	0.163
g_h	0.036

η	Model no. 1 (right)				
	x_α	a	r_α^2	m	θ
0.05	0.09	-0.16	0.22	0.00864	0.98285
.15	.08	-.15	.23	.00781	.94855
.25	.07	-.14	.23	.00718	.91425
.35	.05	-.12	.23	.00658	.87995
.45	.04	-.11	.24	.00602	.84565
.55	.02	-.10	.24	.00554	.81135
.65	.01	-.08	.24	.00510	.77705
.75	-.002	-.07	.24	.00470	.74275
.85	-.02	-.06	.24	.00432	.70845
.95	-.03	-.04	.22	.00394	.67415

Frequency	Model no. 1		Model no. 2		Model no. 3		Model no. 4		Model no. 5	
	Left	Right	Left	Right	Left	Right	Left	Right	Left	Right
f_{h_1}	107	108	102	98	103	102	102	98	102	103
f_{h_2}	501	499	508	470	525	520	510	510	470	480
f_{t_1}	350	339	370	340	342	350	328	342	350	340
f_{α_1}	349	338	369	339	341	349	327	341	349	339
$(\omega_{h_1}/\omega_{\alpha_1})^2$	0.0939	0.1020	0.0763	0.0834	0.0911	0.0853	0.0971	0.0825	0.0853	0.0922
$(\omega_{h_2}/\omega_{\alpha_1})^2$	2.0607	2.1795	1.8953	1.9221	2.3704	2.2201	2.4324	2.2368	1.8136	2.0048

CONFIDENTIAL

CONFIDENTIAL

TABLE I.- Continued

(d) 445 Plan Form

Parameter	Models of Ref. 2, 1 and 2
NACA section	65A004
A	4
Λ, deg	45
λ	0.6
Panel λ	0.657
Span, ft	1.142
A_g	1.65
l, ft	0.630
b_r, ft	0.123
b_s, ft	0.163
g_h	0.030

η	Model of Ref. 2				Model no. 1				θ
	x_α	a	r_α^2	m	x_α	a	r_α^2	m	
0.05	-0.02	-0.07	0.22	0.00561	0.037	-0.117	0.233	0.00733	0.98285
.15	.01	-.10	.22	.00527	.030	-.110	.234	.00648	.94855
.25	.04	-.13	.23	.00493	.023	-.102	.235	.00576	.91425
.35	.07	-.15	.24	.00458	.016	-.095	.236	.00516	.87995
.45	.09	-.18	.24	.00424	.009	-.088	.237	.00472	.84565
.55	.12	-.21	.25	.00389	.002	-.082	.238	.00435	.81135
.65	.15	-.24	.26	.00355	-.005	-.074	.239	.00407	.77705
.75	.17	-.26	.26	.00321	-.012	-.067	.240	.00382	.74275
.85	.20	-.29	.27	.00286	-.018	-.060	.241	.00361	.70855
.95	.23	-.32	.28	.00252	-.025	-.053	.242	.00343	.67415

Frequency	Model of Ref. 2	Model No. 1		Model No. 2	
	Left and right	Left	Right	Left	Right
f_{h_1}	88	67	64	78	73
f_{h_2}	462	357	367	399	387
f_{t_1}	370	356	342	389	378
f_{α_1}	361	356	342	389	378
$(\omega_{h_1}/\omega_{\alpha_1})^2$	0.0594	0.0354	0.0350	0.0402	0.0373
$(\omega_{h_2}/\omega_{\alpha_1})^2$	1.638	1.006	1.151	1.053	1.049

CONFIDENTIAL

TABLE I.- Continued

(e) 452 Plan Form

Parameter	Model of Ref. 2
NACA section	65A004
A	4
Λ, deg	52.5
λ	0.6
Panel λ	0.657
Span, ft	1.142
A_g	1.65
l, ft	0.732
b_r, ft	0.107
b_s, ft	0.163
g_h	0.021

η	Model of Ref. 2				
	x_α	a	r_α^2	m	θ
0.05	0.37	-0.44	0.27	0.00573	0.98285
.15	.30	-.37	.27	.00538	.94855
.25	.24	-.31	.29	.00503	.91425
.35	.17	-.24	.32	.00468	.87995
.45	.11	-.18	.29	.00433	.84565
.55	.04	-.11	.27	.00398	.81135
.65	-0.02	-.05	.27	.00363	.77705
.75	-.09	0.02	.28	.00328	.74275
.85	-.15	.08	.30	.00293	.70845
.95	-.22	.15	.31	.00258	.67415

Frequency	Model of Ref. 2
	Left and right
f_{h_1}	61
f_{h_2}	300
f_{t_1}	370
f_{α_1}	366
$(\omega_{h_1}/\omega_{\alpha_1})^2$	0.0282
$(\omega_{h_2}/\omega_{\alpha_1})^2$	0.6717

TABLE I.- Continued

(f) 460 Plan Form

Parameter	Models 1, 2, 3, 4, and 5
NACA section	65A004
A	4
Λ, deg	60
λ	0.6
Panel λ	0.657
Span, ft	1.142
A_g	1.65
l, ft	0.892
b_r, ft	0.086
b_s, ft	0.163
g_h	0.027

η	Models 1, 2, 3, and 4				Model no. 5				
	x_α	a	${r_\alpha}^2$	m	x_α	a	${r_\alpha}^2$	m	θ
0.05	0.21	-0.31	0.26	0.00465	-0.136	0.040	0.230	0.00730	0.98285
.15	.14	-.23	.24	.00438	-.144	.048	.231	.00668	.94855
.25	.07	-.16	.23	.00410	-.152	.056	.234	.00612	.91425
.35	-.004	-.09	.23	.00383	-.160	.063	.237	.00562	.87995
.45	-.08	-.02	.24	.00356	-.167	.071	.246	.00518	.84565
.55	-.15	.05	.27	.00334	-.175	.079	.257	.00479	.81135
.65	-.22	.12	.30	.00320	-.183	.087	.252	.00442	.77705
.75	-.29	.19	.35	.00314	-.191	.095	.242	.00400	.74275
.85	-.36	.26	.43	.00301	-.199	.103	.235	.00355	.70845
.95	-.43	.33	.51	.00283	-.207	.110	.232	.00305	.67415

Frequency	Model no. 1		Model no. 2		Model no. 3		Model no. 4		Model no. 5	
	Left	Right	Left	Right	Left	Right	Left	Right	Left	Right
f_{h_1}	34.5	34.9	39.5	39.5	39	43.5	41	43	36.5	37.8
f_{h_2}	178	195	193	189	202	210	205	225	175	178
f_{h_3}	——	510	——	——	——	——	——	——	425	410
f_{t_1}	363	370	430	390	390	421	430	435	452	480
f_{α_1}	355	362	421	382	382	412	421	426	423	449
$(\omega_{h_1}/\omega_{\alpha_1})^2$	0.0094	0.0093	0.0088	0.0107	0.0104	0.0111	0.0095	0.0102	0.0065	0.0062
$(\omega_{h_2}/\omega_{\alpha_1})^2$	0.2514	0.2901	0.2101	0.2447	0.2795	0.2598	0.2371	0.2789	0.1063	0.1376
$(\omega_{h_3}/\omega_{\alpha_1})^2$	——	1.984	——	——	——	——	——	——	0.8845	0.7299

TABLE I.- Concluded

(g) 645 Plan Form

Parameter	Model of Ref. 2
NACA section	65A004
A	6.4
Λ, deg	45
λ	0.6
Panel λ	0.646
Span, ft	1.400
A_g	2.75
l, ft	0.813
b_r, ft	0.094
b_s, ft	0.127
g_h	0.013

η	Model of Ref. 2				
	x_α	a	${r_\alpha}^2$	m	θ
0.05	0.15	-0.25	0.26	0.00480	0.98230
.15	.15	-.24	.26	.00437	.94690
.25	.14	-.23	.25	.00404	.91150
.35	.13	-.23	.25	.00381	.87610
.45	.13	-.22	.24	.00362	.84070
.55	.12	-.21	.24	.00335	.80530
.65	.11	-.21	.24	.00302	.76990
.75	.11	-.20	.25	.00266	.73450
.85	.10	-.20	.28	.00243	.69910
.95	.10	-.19	.33	.00226	.66370

Frequency	Model of ref. 2
	Left and right
f_{h_1}	46
f_{h_2}	227
f_{t_1}	522
f_{α_1}	505
$(\omega_{h_1}/\omega_{\alpha_1})^2$	0.0083
$(\omega_{h_2}/\omega_{\alpha_1})^2$	0.2021

TABLE II.- COMPILATION OF ANALYTICAL AND TEST RESULTS

Wing panel behavior code: F – flutter; N – no flutter; D – low damping; E – end of flutter (dynamic pressure increasing); G – strain gages not working; X – wing panel destroyed or not installed

Subscripts: 1 – associated with first occurrence of flutter during the run; 2 – associated with second occurrence of flutter during the run

(a) 245 Plan Form

Model	*Run	**Point	Wing panel behavior		M_e	V_e/V_R	ρ_e, $\frac{\text{slugs}}{\text{cu ft}}$	μ_e	$\sqrt{\mu_e}$	ω_α, $\frac{\text{radians}}{\text{sec}}$	ω_R/ω_α	ω_R, $\frac{\text{radians}}{\text{sec}}$	ω_e, $\frac{\text{radians}}{\text{sec}}$	ω_e/ω_R	V_e, ft/sec	V_R, ft/sec	$\frac{V_e}{b_r\omega_\alpha}$	$\frac{V_R}{b_r\omega_\alpha}$	q_e, lb/ft^2	$\frac{V_e}{b_s\omega_\alpha\sqrt{\mu_e}}$
			Left	Right																
(Ref. 2)	1	1	F_1	G	0.887	1.311	0.0041	12.13	3.48	1665	1.180	1965	1684	0.857	896.0	683.7	4.17	3.18	1646	0.8450
"	2	1	F_1	F_1	.980	1.477	.0047	10.65	3.26	1665	1.198	1995	1797	.901	958.6	648.8	4.46	3.02	2159	.9651
"	3	1	F_1	F_1	1.138	1.567	.0039	12.80	3.58	1665	1.170	1948	1847	.948	1092.7	697.1	5.09	3.25	2328	1.0017
"	4	1	F_1	F_1	1.139	1.447	.0031	16.15	4.02	1665	1.133	1886	1753	.929	1101.3	761.2	5.13	3.54	1862	.8991
"	5	1	F_1	N	1.186	1.558	.0035	14.15	3.76	1665	1.153	1920	1860	.969	1131.7	726.6	5.27	3.38	2241	.9878
"	6	1	F_1	N	1.226	1.601	.0035	14.44	3.80	1665	1.153	1920	1954	1.018	1163.1	726.6	5.42	3.38	2367	1.0045
"	7	1	F_1	N	1.302	1.666	.0035	14.15	3.76	1665	1.153	1920	1973	1.028	1210.7	726.6	5.64	3.38	2565	1.0568
"	8	1	F_1	F_1	1.308	1.732	.0039	12.94	3.60	1665	1.170	1948	1923	.987	1207.7	697.1	5.62	3.25	2844	1.1010
"	9	1	F_1	F_1	1.267	1.673	.0038	13.02	3.61	1665	1.168	1945	2004	1.030	1177.2	703.8	5.48	3.28	2633	1.0702
"	10	1	F_1	F_1	.924	1.333	.0039	12.68	3.56	1665	1.170	1948	1766	.907	929.2	697.1	4.33	3.25	1655	.8566
"	11	1	F_1	X	1.099	1.446	.0033	14.98	3.87	1665	1.145	1906	1784	.936	1074.7	743.3	5.00	3.46	1906	.9114
"	12	1	F_1	F_1	1.099	1.391	.0029	17.32	4.16	1665	1.123	1870	1552	.830	1085.5	780.6	5.05	3.63	1708	.8564

* Run – A run is defined as one operation of the blowdown tunnel from valve opening to valve closing.

** Point – Chronological order in which recorded points occurred during the test run.

TABLE II.- Continued

(b) 400 Plan Form

Model	Run	Point	Wing panel behavior Left	Wing panel behavior Right	M_e	V_e/V_R	ρ_e slugs/cu ft	μ_e	$\sqrt{\mu_e}$	ω_α radians/sec	ω_R/ω_α	ω_R radians/sec	ω_e radians/sec	ω_e/ω_R	V_e ft/sec	V_R ft/sec	$\frac{V_e}{b_r\omega_\alpha}$	$\frac{V_R}{b_r\omega_\alpha}$	q_e lb/ft^2	$\frac{V_e}{b_s\omega_\alpha\sqrt{\mu_e}}$
(Ref. 2)	1	1	N	D_1	0.890	0.961	0.0031	28.32	5.32	2526	—	—	—	—	877.0	914.1	2.133	2.22	1184.4	0.3547
"		2	N	F_1	.919	.997	.0031	28.06	5.30	2526	0.3550	896.7	1058	1.180	902.9	905.8	2.192	2.20	1263.1	.4138
"	2	1	N	D_1	.886	.970	.0031	27.89	5.28	2526	—	—	—	—	874.8	901.7	2.125	2.19	1193.2	.4024
"		2	N	F_1	.908	.991	.0032	27.44	5.24	2526	.3480	879.0	1062	1.208	889.3	897.6	2.159	2.18	1253.1	.4122
"	3	1	N	D_1	.917	.956	.0028	30.77	5.55	2526	—	—	—	—	901.1	942.9	2.189	2.29	1147.4	.3943
"		2	N	F_1	.986	1.021	.0028	30.58	5.53	2526	.3628	916.4	—	—	958.3	938.7	2.327	2.28	1305.8	.4209
"	4	1	N	D_1	.955	.973	.0027	32.21	5.68	2526	—	—	—	—	941.2	967.6	2.290	2.33	1196.0	.4024
"		2	N	F_1	.949	.990	.0029	30.36	5.51	2526	.3725	940.9	1070	1.137	933.8	942.9	2.268	2.29	1264.4	.4116
"	5	1	D_1	N	.984	.948	.0024	36.24	6.02	2526	—	—	—	—	968.3	1021.1	2.350	2.45	1125.0	.3906
"		2	F_1	N	1.027	.991	.0025	35.13	5.93	2526	.4002	1010.9	1057	1.046	1000.0	1008.8	2.429	2.45	1250.0	.4096
"	6	1	N	D_1	1.336	1.270	.0028	31.02	5.57	2526	—	—	—	—	1208.0	951.1	2.934	2.31	2043.0	.5267
"		2	D_1	D_1	1.333	1.340	.0032	27.14	5.21	2526	—	—	—	—	1197.2	893.5	2.908	2.17	2293.3	.5581
"		3	D_1	F_1	1.338	1.335	.0032	27.30	5.22	2526	.3533	892.4	1416	1.587	1198.7	897.6	2.911	2.18	2299.0	.5577
"		4	F_1	F_1	1.318	1.370	.0035	24.92	4.99	2526	.3378	853.3	1375	1.611	1179.0	860.5	2.863	2.09	2432.6	.5738
"	7	1	D_1	D_1	.941	.938	.0026	33.39	5.78	2526	—	—	—	—	923.0	984.1	2.242	2.39	1107.5	.3878
"		2	N	F_1	1.051	1.025	.0026	33.41	5.78	2526	.3903	985.9	1414	1.434	1008.7	984.1	2.450	2.39	1322.7	.4238
"		3	D_1	E_1	1.154	1.121	.0027	32.17	5.67	2526	—	—	—	—	1085.0	967.6	2.635	2.35	1589.3	.4648
"		4	D_1	F_2	1.227	1.253	.0032	27.15	5.21	2526	.3527	890.9	1257	1.411	1119.3	893.5	2.718	2.17	2004.5	.5218
"	8	1	D_1	D_1	1.034	1.015	.0025	34.75	5.89	2526	—	—	—	—	1015.6	1000.5	2.467	2.43	1289.3	.4188
"		2	D_1	F_1	1.100	1.081	.0026	33.45	5.78	2526	.3902	985.6	1204	1.222	1063.5	984.1	2.583	2.39	1470.3	.4469
"		3	F_1	F_1	1.227	1.255	.0030	28.99	5.38	2526	—	—	—	—	1152.8	918.2	2.800	2.23	1993.4	.5217
"	9	1	F_1	N	1.009	1.039	.0029	30.16	5.49	2526	.3710	937.1	1126	1.202	975.5	938.8	2.369	2.28	1379.8	.4316
"	10	1	F_1	N	.950	.979	.0028	31.10	5.58	2526	.3770	952.3	1100	1.155	934.1	951.1	2.262	2.31	1214.5	.4066
"	11	1	D_1	N	.878	.978	.0033	26.32	5.13	2526	—	—	—	—	861.7	881.1	2.093	2.14	1225.2	.4080
"		2	F_1	N	.926	1.031	.0034	25.52	5.05	2526	.3418	863.4	1156	1.339	899.8	872.9	2.185	2.12	1376.4	.4327
"	12	1	D_1	X	.863	.912	.0028	31.02	5.57	2526	—	—	—	—	867.5	951.1	2.107	2.31	1053.6	.3783
"		2	F_1	X	.949	.990	.0029	29.82	5.46	2526	.3692	932.6	1112	1.192	925.7	934.6	2.248	2.27	1242.5	.4118
"	13	1	F_1	X	1.017	1.014	.0026	33.33	5.77	2526	.3898	984.6	1125	1.142	993.3	979.9	2.412	2.38	1282.6	.4181
"	14	1	D_1	X	.930	.948	.0027	32.17	5.67	2526	—	—	—	—	917.3	967.6	2.228	2.35	1135.9	.3929
"		2	F_1	X	1.017	1.008	.0027	32.66	5.71	2526	.3855	973.8	1125	1.155	983.2	975.8	2.388	2.37	1305.0	.4182
"	15	1	D_1	X	1.284	1.324	.0034	25.58	5.06	2526	—	—	—	—	1156.1	872.9	2.808	2.12	2272.2	.5549
"		2	F_1	X	1.259	1.391	.0039	22.30	4.72	2526	.3200	808.3	1423	1.760	1134.1	815.2	2.754	1.98	2508.1	.5836
"	16	1	F_1	X	.988	.983	.0026	32.86	5.73	2526	.3870	977.6	1145	1.171	958.9	975.8	2.329	2.37	1195.3	.4064
"		2	D_2	X	1.267	1.260	.0030	28.95	5.38	2526	—	—	—	—	1161.8	922.3	2.822	2.24	2024.7	.5245
"		3	F_2	X	1.262	1.280	.0031	27.66	5.26	2526	.3560	899.3	1348	1.499	1154.0	901.7	2.803	2.19	2064.2	.5328
"	17	1	F_1	X	1.052	1.014	.0025	34.43	5.87	2526	.3960	1000.3	1149	1.149	1014.4	1000.5	2.464	2.43	1286.3	.4197
"	18	1	D_1	X	1.348	1.420	.0036	24.13	4.91	2526	—	—	—	—	1204.2	848.2	2.925	2.06	2610.2	.5956
"		2	F_1	X	1.328	1.471	.0040	21.74	4.66	2526	.3160	798.2	1494	1.872	1187.4	807.0	2.884	1.96	2819.8	.6188
"	19	1	D_1	X	1.411	1.387	.0029	29.95	5.47	2526	—	—	—	—	1296.7	934.6	3.149	2.27	2438.1	.5757
"		2	F_1	X	1.383	1.444	.0033	26.36	5.13	2526	.3475	877.8	1466	1.670	1272.5	881.1	3.091	2.14	2671.8	.6024
1	20	1	F_1	X	.920	1.001	.0025	35.45	5.95	2422	.4015	972.4	1112	1.144	971.2	970.6	2.460	2.46	1179.0	.4134
1	21	1	F_1	X	.943	.996	.0024	36.74	6.06	2422	.4090	990.6	1081	1.091	982.7	986.4	2.489	2.50	1158.8	.4108
1	22	1	D_1	X	1.032	1.004	.0021	42.34	6.51	2422	.4388	1062.8	1125	1.059	1058.1	1053.4	2.680	2.67	1175.8	.4117
1		2	F_1	X	1.145	1.079	.0020	43.40	6.59	2422	.4440	1075.4	1125	1.046	1149.2	1065.3	2.911	2.70	1320.7	.4417
1	23	1	D_1	X	1.050	1.024	.0021	41.81	6.47	2422	—	—	—	—	1070.2	1045.5	2.711	2.65	1202.6	.4190
1		2	F_1	X	1.105	1.059	.0021	42.34	6.51	2422	.4388	1062.8	1106	1.041	1115.6	1053.4	2.826	2.67	1306.8	.4341
1	24	1	D_1	X	.875	.976	.0026	33.50	5.79	2422	—	—	—	—	920.1	943.0	2.331	2.39	1100.6	.4025
1		2	F_1	X	.904	1.006	.0026	33.13	5.76	2422	.3890	942.2	1081	1.147	945.0	939.0	2.394	2.38	1160.9	.4156
1	25	1	F_1	X	.865	1.013	.0029	30.10	5.49	2422	.3708	898.1	1175	1.308	907.3	895.6	2.298	2.27	1193.6	.4186
1	26	1	F_1	X	1.301	1.282	.0024	36.59	6.05	2422	.4080	988.2	1282	1.297	1259.6	982.4	3.191	2.49	1903.9	.5274
2	27	1	N	D_1	1.333	1.426	.0029	29.98	5.48	2422	—	—	—	—	1277.1	895.6	3.235	2.27	2364.9	.5903
2		2	N	F_1	1.328	1.476	.0032	27.48	5.24	2422	.3545	858.6	1319	1.536	1269.7	860.1	3.216	2.18	2579.4	.6138

TABLE II.- Continued

(c) 430 Plan Form

Model	Run	Point	Wing panel behavior: Left	Wing panel behavior: Right	M_e	V_e/V_R	ρ_e, slugs/cu ft	μ_e	$\sqrt{\mu_e}$	ω_α, radians/sec	ω_R/ω_α	ω_R, radians/sec	ω_e, radians/sec	ω_e/ω_R	V_e, ft/sec	V_R, ft/sec	$\frac{V_e}{b_r\omega_\alpha}$	$\frac{V_R}{b_r\omega_\alpha}$	q_e, lb/ft^2	$\frac{V_e}{b_s\omega_\alpha\sqrt{\mu_e}}$
1	1	1	D_1	D_1	0.774	1.074	0.0030	40.07	6.33	2159	—	—	—	—	816.4	759.8	2.538	2.362	1000	0.3665
1		2	F_1	F_1	.796	1.121	.0032	38.17	6.18	2159	0.5373	1160	1100	0.948	836.0	745.7	2.599	2.318	1118	.3844
1	2	1	D_1	D_1	1.369	1.763	.0035	34.90	5.91	2159	—	—	—	—	1268.5	719.6	3.943	2.237	2816	.6099
1		2	F_1	F_1	1.360	1.891	.0044	27.76	5.27	2159	.5588	1206	1596	1.323	1246.0	658.8	3.873	2.048	3416	.6718
1	3	1	F_1	F_1	.899	1.140	.0025	48.86	6.99	2159	.5188	1120	993	.887	937.4	822.2	2.914	2.556	1098	.3811
1		2	E_1	E_1	.963	1.199	.0025	48.86	6.99	2159	.5188	1120	—	—	986.1	822.2	3.065	2.556	1215	.4009
1		3	D_2	D_2	1.168	1.553	.0032	38.17	6.18	2159	—	—	—	—	1157.0	745.0	3.597	2.316	2142	.5320
1		4	F_2	F_2	1.158	1.623	.0037	33.01	5.74	2159	.5478	1183	1433	1.211	1142.9	704.2	3.553	2.189	2416	.5658
1	4	1	F_1	F_1	.913	1.100	.0022	55.52	7.45	2159	—	—	942	—	952.4	866.0	2.961	2.692	998	.3633
1		2	E_1	E_1	.959	1.148	.0022	55.52	7.45	2159	—	—	—	—	994.4	866.0	3.091	2.692	1088	.3793
1		3	D_2	D_2	1.249	1.634	.0032	38.17	6.18	2159	—	—	—	—	1217.4	745.0	3.784	2.316	2371	.5598
1		4	F_2	F_2	1.251	1.727	.0037	33.01	5.74	2159	.5478	1183	1451	1.226	1216.2	704.2	3.781	2.189	2736	.6021
1	5	1	G	F_1	.850	1.135	.0029	42.11	6.49	2125	.5303	1127	1024	.909	865.1	762.4	2.732	2.408	1085	.3848
1		2	G	E_1	.884	1.172	.0029	42.11	6.49	2125	.5303	1127	—	—	893.4	762.4	2.822	2.408	1157	.3974
2	6	1	F_1	F_1	.850	1.068	.0026	46.98	6.85	2227	.5217	1161.8	1037	.892	894.0	834.9	2.694	2.516	1039	.3595
2	7	1	F_1	F_1	.820	1.034	.0026	46.98	6.85	2227	.5217	1161.8	999	.960	863.0	834.9	2.601	2.516	968	.3471
2	8	1	F_1	F_1	.855	1.027	.0023	53.11	7.29	2227	.5141	1145	955	.834	900.3	877.0	2.713	2.643	932	.3261
2		2	E_1	E_1	.947	1.120	.0023	53.11	7.29	2227	.5141	1145	—	—	984.0	877.0	2.643	2.643	1115	.3402
2		3	N	F_2	1.227	1.669	.0034	35.93	5.99	2131	.5418	1154.6	1433	1.241	1199.0	718.2	3.776	2.262	2444	.5763
2		4	D_2	F_2	1.219	1.620	.0041	29.79	5.46	2319	—	—	—	—	1178.4	727.3	3.410	2.105	2847	.5710
2		5	F_2	F_2	1.235	1.732	.0049	24.93	4.99	2319	.5656	1311.6	1571	1.198	1177.6	680.0	3.408	1.968	3398	.6243
2	9	1	F_1	G	.833	.997	.0025	48.86	6.99	2319	.5188	1203.1	968	.804	884.0	883.2	2.558	2.556	977	.3346
2		2	E_1	G	.994	1.192	.0027	45.24	6.73	2319	.5248	1217.0	—	—	1024.0	855.9	2.964	2.477	1416	.4025
2		3	D_2	G	1.129	1.461	.0035	34.90	5.91	2319	—	—	—	—	1129.3	773.0	3.268	2.237	2232	.5055
2		4	F_2	G	1.130	1.544	.0041	29.79	5.46	2319	.5543	1285.4	1458	1.134	1123.4	727.3	3.251	2.105	2587	.5443
2	10	1	F_1	G	.848	1.012	.0025	48.86	6.99	2319	.5186	1203	999	.830	894	883.2	2.587	2.556	999	.3384
2		2	E_1	G	.995	1.186	.0027	45.24	6.73	2319	.5246	1216	—	—	1018	855.9	2.946	2.477	1399	.4002
2		3	D_2	G	1.088	1.353	.0031	39.40	6.28	2319	—	—	—	—	1096	810.3	3.172	2.345	1862	.4617
2		4	F_2	G	1.095	1.437	.0036	33.93	5.82	2319	.5458	1266	1389	1.097	1099	764.7	3.181	2.213	2174	.4996
2	11	1	F_1	F_1	.814	1.035	.0026	46.98	6.85	2227	.5217	1162	1005	.865	864	834.9	2.604	2.516	970	.3475
2	12	1	F_1	X	.885	1.040	.0024	50.90	7.13	2319	.5152	1195	930	.778	934	898.0	2.703	2.599	1047	.3466
2		2	E_1	X	.930	1.086	.0024	50.90	7.13	2319	.5152	1195	—	—	975	898.0	2.822	2.599	1141	.3618
2		3	D_2	X	1.172	1.449	.0032	38.17	6.18	2319	—	—	—	—	1160	800.6	3.357	2.317	2153	.4966
2		4	F_2	X	1.161	1.533	.0038	32.14	5.67	2319	.5493	1274	1363	1.070	1147	748.4	3.320	2.166	2500	.5352
3	13	1	D_1	D_1	.746	1.055	.0031	39.43	6.28	2169	—	—	—	—	800.0	758.2	2.475	2.346	992	.3603
3		2	F_1	F_1	.750	1.081	.0034	35.95	6.00	2169	.5416	1175	1068	.909	791.1	732.0	2.448	2.265	1064	.3729
4	14	1	F_1	F_1	.780	1.045	.0026	46.97	6.85	2100	.5216	1095	1056	.964	822.7	786.9	2.629	2.515	880	.3509
5	15	1	D_1	D_1	.785	1.118	.0034	35.95	6.00	2159	—	—	—	—	814.8	728.6	2.535	2.267	1129	.3861
5		2	F_1	F_1	.812	1.163	.0035	34.92	5.91	2159	.5416	1169.3	1097	.938	837.5	719.9	2.603	2.238	1227	.3966

CONFIDENTIAL

TABLE II.- Continued

(d) 445 Plan Form

Model	Run	Point	Wing panel behavior		M_e	V_e/V_R	ρ_e, $\frac{slugs}{cu\ ft}$	μ_e	$\sqrt{\mu_e}$	ω_α, $\frac{radians}{sec}$	ω_R/ω_α	ω_R, $\frac{radians}{sec}$	ω_e, $\frac{radians}{sec}$	ω_e/ω_R	V_e, ft/sec	V_R, ft/sec	$\frac{V_e}{b_r\omega_\alpha}$	$\frac{V_R}{b_r\omega_\alpha}$	q_e, lb/ft^2	$\frac{V_e}{b_s\omega_\alpha\sqrt{\mu_e}}$
			Left	Right																
(Ref. 2)	1	1	F_1	F_1	0.813	1.032	0.0033	37.10	6.09	2268	0.5295	1201.5	1047	0.871	805.4	780.4	2.88	2.80	1070	0.3577
"	2	1	F_1	F_1	.797	1.039	.0031	39.49	6.28	2268	.5245	1200.9	1047	.872	795.6	765.8	2.85	2.75	981	.3427
"	3	1	F_1	F_1	.863	1.036	.0028	43.72	6.61	2268	.5160	1170.3	995	.850	856.0	825.8	3.06	2.96	1026	.3503
"	4	1	F_1	F_1	.863	1.030	.0028	43.72	6.61	2268	.5160	1170.3	—	—	850.7	825.8	3.04	2.96	1013	.3481
"	5	1	F_1	F_1	.906	1.047	.0026	47.08	6.86	2268	.5095	1155.5	995	.861	887.7	848.1	3.18	3.04	1024	.3500
"	6	1	F_1	F_1	.904	1.062	.0027	45.34	6.73	2268	.5128	1163.0	958	.824	888.8	837.0	3.19	3.00	1067	.3572
"	7	1	N	D_1	1.396	1.587	.0029	42.21	6.50	2268	.5192	1177.5	—	—	1296.7	817.4	4.65	2.93	2439	.5396
"		2	N	F_1	1.376	1.641	.0034	36.01	6.00	2268	.5322	1207.0	1585	1.313	1267.8	772.7	4.55	2.77	2732	.5716
"		3	D_1	F_1	1.326	1.800	.0048	25.50	5.05	2268	.5569	1263.0	—	—	1215.0	675.1	4.36	2.42	2067	.6508
"		4	F_1	F_1	1.340	1.830	.0054	22.67	4.76	2268	.5643	1279.8	1755	1.371	1214.8	663.9	4.36	2.38	3984	.6903
"	8	1	N	F_1	1.023	1.095	.0021	59.73	7.73	2268	.4870	1104.5	1119	1.013	1011.0	923.0	3.62	3.32	1073	.3538
"		2	N	F_2	1.361	1.614	.0033	36.88	6.07	2268	.5302	1202.4	1540	1.281	1256.0	778.0	4.50	2.79	2603	.5597
"	9	1	F_1	F_1	.975	1.124	.0024	51.23	7.16	2268	.5016	1137.6	1121	.985	981.0	873.0	3.51	3.13	1155	.3706
"		2	F_1	E_1	1.301	1.540	.0031	38.99	6.24	2268	.5255	1191.8	—	—	1224.0	795.0	4.38	2.84	2322	.5306
"	10	1	F_1	F_1	.975	1.125	.0025	49.77	7.05	2268	.5047	1144.6	1023	.894	973.0	865.0	3.48	3.10	1183	.3733
"	11	1	F_1	F_1	.924	1.052	.0026	47.08	6.86	2268	.5095	1155.5	1040	.900	921.0	875.0	3.30	3.04	1103	.3632
"	12	1	F_1	F_1	.794	.972	.0028	43.72	6.61	2268	.5160	1170.3	1063	.908	803.3	825.8	2.88	2.96	903	.3287
"	13	1	N	F_1	.961	1.065	.0022	55.64	7.46	2268	.4938	1120.0	1096	.978	956.0	901.1	3.42	3.23	1005	.3466
"		2	N	F_2	1.342	1.600	.0035	34.98	5.92	2268	.5342	1212.0	1570	1.295	1223.0	764.4	4.38	2.74	2618	.5588
1	14	1	N	F_1	.940	1.059	.0018	80.93	9.00	2149	.4019	863.6	859	.995	977.0	922.4	3.69	3.49	860	.3099
1		2	N	E_1	1.039	1.129	.0017	85.69	9.26	2149	—	—	—	—	1062.0	940.9	4.01	3.56	952	.3274
1	15	1	N	F_1	.862	1.007	.0019	76.67	8.76	2149	.4078	876.3	856	.980	908.0	901.3	3.43	3.41	768	.2959
1		2	N	E_1	1.049	1.140	.0017	85.69	9.26	2149	—	—	—	—	1073.0	940.9	4.06	3.56	1004	.3308
1	16	1	F_1	F_1	.871	1.041	.0024	60.70	7.79	2195	.4325	949.3	919	.968	882.0	847.5	3.27	3.14	922	.3164
1		2	G	E_1	1.175	1.336	.0020	72.84	8.53	2149	—	—	—	—	1183.0	885.4	4.48	3.35	1426	.3960
1		3	G	D_2	1.293	1.705	.0037	39.37	6.27	2149	.4713	1012.7	—	—	1217.0	713.6	4.60	2.70	2753	.5542
1		4	G	F_2	1.292	1.741	.0038	38.34	6.19	2149	.4736	1017.7	1460	1.435	1233.0	708.3	4.66	2.68	2920	.5687
1	17	1	F_1	G	.830	1.044	.0026	56.03	7.49	2237	.4402	984.6	982	.997	879.0	841.9	3.19	3.06	996	.3219
2	18	1	D_1	G	1.348	1.643	.0041	35.53	5.96	2444	—	—	—	—	1289.0	784.7	4.29	2.61	3411	.5429
2		2	F_1	G	1.346	1.712	.0049	29.73	5.45	2444	.4925	1203.8	1591	1.322	1271.0	742.6	4.23	2.47	3979	.5854
2	19	1	D_1	G	1.219	1.423	.0033	44.15	6.64	2444	—	—	—	—	1202.0	844.8	4.00	2.81	2388	.4544
2		2	F_1	G	1.192	1.445	.0037	39.37	6.27	2444	.4712	1151.7	1302	1.130	1173.0	811.7	3.90	2.70	2537	.4696
2	20	1	D_1	G	1.204	1.411	.0033	44.15	6.64	2444	—	—	—	—	1192.0	844.8	3.96	2.81	2328	.4506
2		2	F_1	G	1.186	1.464	.0039	37.35	6.11	2444	.4756	1162.4	1353	1.164	1166.0	804.4	3.88	2.68	2628	.4790
2	21	1	F_1	G	.836	1.063	.0025	58.27	7.63	2444	.4369	1067.9	900	.843	997.0	929.0	3.32	3.09	1104	.3280
2	22	1	N	D_1	1.307	1.600	.0037	39.37	6.27	2375	.4713	1119.3	—	—	1262.0	788.8	4.32	2.70	2946	.5199
2		2	N	F_1	1.332	1.682	.0044	33.11	5.75	2375	.4848	1151.4	1539	1.337	1253.1	744.9	4.29	2.55	3454	.5629
2	23	1	F_1	F_1	.882	.980	.0022	66.22	8.14	2410	.4237	1021.1	905	.886	939.8	960.0	3.17	3.24	971	.2939
2		2	E_1	E_1	1.149	1.183	.0020	72.84	8.53	2410	—	—	—	—	1173.9	993.0	3.96	3.35	1378	.3503
2		3	N	D_2	1.285	1.528	.0033	44.15	6.64	2375	.4618	1096.8	—	—	1254.0	820.9	4.29	2.81	2595	.4878
2		4	N	F_2	1.283	1.591	.0038	38.34	6.19	2375	.4736	1124.8	1495	1.329	1245.8	782.9	4.26	2.68	2949	.5199
2	24	1	F_1	F_1	.854	1.037	.0028	52.03	7.21	2410	.4475	1078.5	955	.885	912.8	880.0	3.08	2.97	1166	.3223
2	25	1	F_1	F_1	.908	1.033	.0024	60.70	7.79	2410	.4326	1142.6	930	.892	961.3	931.0	3.24	3.14	1109	.3141
2		2	E_1	G	1.085	1.184	.0023	63.34	7.96	2410	—	—	—	—	1116.1	943.0	3.76	3.18	1432	.3569
2		3	D_2	G	1.142	1.242	.0026	56.03	7.49	2444	.4402	1075.9	—	—	1142.3	920.0	3.80	3.06	1696	.3828
2		4	F_2	G	1.176	1.306	.0028	52.03	7.21	2444	.4475	1093.8	1115	1.019	1166.4	892.9	3.88	2.97	1905	.4060
2	26	1	F_1	G	.874	.997	.0025	58.27	7.63	2444	.4367	1067.4	892	.836	926.3	929.0	3.08	3.09	1072	.3047
2	27	1	F_1	G	.920	.994	.0022	66.22	8.14	2444	.4236	1035.4	817	.789	967.7	974.1	3.22	3.24	1030	.2984
2		2	E_1	G	1.055	1.097	.0021	69.37	8.33	2444	—	—	—	—	1085.3	989.1	3.61	3.29	1237	.3270
2	28	1	D_1	G	1.212	1.450	.0035	41.62	6.45	2444	.4665	1140.2	—	—	1199.2	826.8	3.99	2.75	2517	.4667
2		2	F_1	G	1.219	1.508	.0039	37.35	6.11	2444	.4755	1162.2	1345	1.157	1201.6	796.7	4.00	2.65	2815	.4936
2	29	1	F_1	G	.846	.960	.0024	60.70	7.79	2444	.4324	1056.9	886	.838	906.2	944.0	3.01	3.14	985	.2920
2	30	1	F_1	G	.877	.992	.0024	60.70	7.79	2444	.4324	1056.9	898	.850	936.4	944.0	3.11	3.14	1052	.3017

CONFIDENTIAL

CONFIDENTIAL

TABLE II.- Continued

(e) 452 Plan Form

Model	Run	Point	Wing panel behavior		M_e	V_e/V_R	ρ_e, $\frac{\text{slugs}}{\text{cu ft}}$	μ_e	$\sqrt{\mu_e}$	ω_α, $\frac{\text{radians}}{\text{sec}}$	ω_R/ω_α	ω_R, $\frac{\text{radians}}{\text{sec}}$	ω_e, $\frac{\text{radians}}{\text{sec}}$	ω_e/ω_R	V_e, ft/sec	V_R, ft/sec	$\frac{V_e}{b_r\omega_\alpha}$	$\frac{V_R}{b_r\omega_\alpha}$	q_e, lb/ft^2	$\frac{V_e}{b_s\omega_\alpha\sqrt{\mu_e}}$
			Left	Right																
(Ref. 2)	1	1	N	F_1	0.817	0.916	0.0032	51.59	7.18	2300	0.4748	1092	1005	0.920	847.7	925.3	3.44	3.76	1150	0.3149
"		2	D_1	F_1	.824	.938	.0035	47.59	6.90	2300	.4830	1111	—	—	845	901	3.43	3.66	1250	.3266
"		3	F_1	F_1	.821	.951	.0037	44.26	6.66	2300	.4900	1127	999	.886	835	878	3.39	3.57	1290	.3344
"	2	1	F_1	F_1	.900	.963	.0029	57.36	7.57	2300	.4638	1067	906	.849	924.7	959.8	3.76	3.90	1240	.3258
"	3	1	D_1	G	.932	.967	.0027	60.26	7.76	2300	.4582	1054	—	—	945.2	977	3.84	3.97	1206	.3249
"		2	F_1	G	1.001	1.038	.0028	59.24	7.70	2300	.4600	1058	964	.911	1006.5	969.6	4.09	3.94	1418	.3487
"	4	1	F_1	G	1.118	1.023	.0021	77.31	8.79	2300	—	—	—	—	1089.7	1065.6	4.43	4.33	1247	.3307
"		2	E_1	G	1.290	1.126	.0020	81.12	9.01	2300	—	—	—	—	1222.5	1085.3	4.97	4.41	1494	.3619
"		3	D_2	G	1.386	1.275	.0027	61.67	7.86	2300	.4554	1047	—	—	1255	984	5.10	4.00	2126	.4259
"		4	F_2	G	1.412	1.297	.0027	60.99	7.82	2300	.4565	1050	1136	1.082	1271	980	5.16	3.98	2181	.4335
"	5	1	F_1	G	1.123	1.042	.0022	75.51	8.69	2300	.4313	992	1005	1.013	1102.7	1058.2	4.48	4.30	1338	.3385
"		2	E_1	G	1.200	1.082	.0021	78.83	8.88	2300	—	—	—	—	1163.4	1075.5	4.73	4.37	1421	.3495
"		3	D_2	G	1.356	1.270	.0027	60.68	7.79	2300	.4573	1052	—	—	1244.3	979.5	5.06	3.98	2090	.4261
"		4	F_2	G	1.419	1.316	.0027	60.21	7.76	2300	.4582	1054	1120	1.063	1285.6	977	5.22	3.97	2231	.4419
"	6	1	D_1	G	1.006	.993	.0024	67.24	8.20	2300	.4455	1025	—	—	1009.5	1016.4	4.10	4.13	1223	.3284
"		2	F_1	G	1.066	1.038	.0025	67.19	8.20	2300	.4455	1025	916	.894	1055.4	1016.4	4.29	4.13	1392	.3433
"	7	1	D_1	G	.991	.980	.0024	67.77	8.23	2300	.4445	1022	—	—	998.1	1018.9	4.06	4.14	1195	.3235
"		2	F_1	G	1.103	1.062	.0024	69.16	8.32	2300	.4420	1017	942	.926	1089.9	1026.2	4.43	4.17	1425	.3494
"	8	1	F_1	N	1.285	1.123	.0022	75.27	8.68	2300	.4315	992	—	—	1185.2	1055.8	4.82	4.29	1545	.3642
"	9	1	F_1	N	1.189	1.082	.0024	68.96	8.30	2300	.4425	1018	1062	1.043	1107.3	1023.8	4.50	4.16	1471	.3558
"		2	F_1	F_1	1.223	1.122	.0025	65.30	8.08	2300	.4490	1033	1100	1.065	1127	1004.1	4.58	4.08	1588	.3720
"	10	1	F_1	F_1	1.006	1.016	.0029	56.24	7.50	2300	.4657	1071	1068	.997	967.7	952.4	3.93	3.87	1358	.3442
"	11	1	F_1	F_1	1.023	1.030	.0030	55.32	7.44	2300	.4674	1075	1062	.988	975.7	947.5	3.96	3.85	1428	.3498
"	12	1	F_1	F_1	1.097	1.041	.0026	64.15	8.01	2300	.4510	1037	1049	1.012	1037.5	996.7	4.22	4.05	1399	.3455
"	13	1	F_1	F_1	.660	.894	.0066	24.95	5.00	2300	—	—	1144	—	653	730.9	2.65	2.97	1407	.3484
"		2	G	F_1	.797	.941	.0042	39.43	6.28	2300	.5008	1152	1037	.900	794.1	844.1	3.23	3.43	1324	.3373

CONFIDENTIAL

CONFIDENTIAL

TABLE II.- Continued

(f) 460 Plan Form

Model	Run	Point	Wing panel behavior Left	Wing panel behavior Right	M_e	V_e/V_R	ρ_e slugs/cu ft	μ_e	$\sqrt{\mu_e}$	ω_α radians/sec	ω_R/ω_α	ω_R radians/sec	ω_e radians/sec	ω_e/ω_R	V_e ft/sec	V_R ft/sec	$\frac{V_e}{b_r\omega_\alpha}$	$\frac{V_R}{b_r\omega_\alpha}$	q_e lb/ft^2	$\frac{V_e}{b_s\omega_\alpha\sqrt{\mu_e}}$
1	1	1	F_1	N	1.316	1.114	0.0020	—	—	—	—	—	—	—	1222.2	1097	—	—	—	—
1		2	F_1	F_1	1.304	1.121	.0020	120.19	10.96	2255	0.3104	700	804.2	1.149	1213.4	1082.1	6.26	5.58	1472	0.3012
1	2	1	F_1	N	1.003	1.001	.0029	86.16	9.28	2276	.3378	768.8	791.7	1.030	985.7	984.6	5.04	5.03	1409	.2863
1	3	1	F_1	N	.986	.986	.0028	86.37	9.29	2276	.3377	768.6	779.1	1.014	970.6	984.6	4.96	5.03	1319	.2816
1		2	F_1	D_1	1.019	1.025	.0029	85.20	9.23	2255	.3387	763.8	—	—	996.1	971.6	5.14	5.01	1439	.2936
1		3	F_1	F_1	1.032	1.037	.0029	84.61	9.20	2255	.3393	765.1	776.6	1.002	1005.3	969.7	5.18	5.00	1465	.2973
1	4	1	F_1	D_1	.959	.981	.0030	82.40	9.08	2255	.3412	769.4	760.3	.988	945.6	963.8	4.88	4.97	1341	.2833
1		2	F_1	F_1	.989	1.009	.0030	81.42	9.02	2255	.3422	771.7	760.3	.985	968.9	960	5.00	4.95	1408	.2922
1	5	1	F_1	N	.960	.972	.0030	82.26	9.07	2276	.3414	777	716.3	.922	945.1	972.8	4.83	4.97	1340	.2809
1		2	F_1	F_1	.960	.982	.0030	82.51	9.08	2255	.3412	769.4	716.3	.931	946.5	963.8	4.88	4.97	1344	.2836
1	6	1	F_1	F_1	.918	.951	.0030	81.99	9.05	2255	.3418	770.8	678.6	.880	914.7	961.9	4.72	4.96	1255	.2750
2	7	1	N	F_1	1.039	1.047	.0032	75.83	8.71	2399	.3344	802.2	851.4	1.061	995.6	951.1	4.83	4.61	1586	.2923
2		2	F_1	F_1	1.076	1.043	.0032	76.73	8.76	2522	.3240	817.1	873.4	1.069	1022.7	980.3	4.72	4.52	1673	.2840
2	8	1	F_1	F_1	.985	.970	.0031	78.78	8.88	2522	.3222	812.6	873.4	1.075	961.7	991.2	4.43	4.57	1434	.2634
2	9	1	N	F_1	1.068	1.039	.0030	80.83	8.99	2399	.3300	791.7	823.1	1.040	1008	969.7	4.89	4.70	1524	.2867
2		2	F_1	F_1	1.062	1.012	.0031	78.95	8.89	2522	.3200	812.1	873.4	1.075	1003.3	991.2	4.63	4.57	1560	.2745
2	10	1	F_1	F_1	1.286	1.050	.0021	115.17	10.73	2522	.2945	742.7	829.4	1.117	1179.3	1123.5	5.44	5.18	1460	.2674
2	11	1	N	F_1	1.120	1.034	.0027	89.88	9.48	2399	.3223	773.2	823.1	1.065	1039.8	1005.8	5.04	4.87	1460	.2805
2		2	D_1	F_1	1.127	1.021	.0028	86.80	9.32	2522	.3155	795.7	—	—	1043.5	1021.6	4.81	4.71	1524	.2724
2		3	F_1	F_1	1.127	1.023	.0028	87.04	9.33	2522	.3153	795.2	867.1	1.090	1045	1021.6	4.82	4.71	1529	.2724
2	12	1	N	F_1	1.103	1.061	.0030	80.83	8.99	2399	.3300	791.7	829.4	1.048	1028.5	969.7	4.99	4.70	1587	.2926
2		2	D_1	F_1	1.103	1.031	.0030	80.83	8.99	2522	.3206	808.6	—	—	1028.5	997.7	4.74	4.60	1587	.2783
2		3	F_1	F_1	1.103	1.031	.0030	80.83	8.99	2522	.3206	808.6	873.4	1.080	1028.5	997.7	4.74	4.60	1587	.2974
2	13	1	F_1	N	1.178	1.003	.0025	99.66	9.98	2645	.2967	784.8	860.8	1.097	1099.3	1096.4	4.83	4.82	1511	.2555
2	14	1	F_1	F_1	.821	.902	.0050	49.28	7.02	2522	.3500	882.7	867.1	.982	772.6	856.7	3.56	3.95	1492	.2677
2	15	1	D_1	G	1.356	1.039	.0020	124.64	11.16	2645	—	—	—	—	1226.5	1180.6	5.39	5.19	1504	.2549
2		2	F_1	G	1.374	1.049	.0020	123.77	11.13	2645	.2800	740.6	873.4	1.179	1238.4	1180.6	5.44	5.19	1534	.2581
2	16	1	D_1	G	1.262	1.004	.0021	117.71	10.85	2645	.2840	751.2	—	—	1164.7	1160.1	5.12	5.10	1424	.2490
2		2	F_1	G	1.294	1.037	.0022	113.16	10.64	2645	.2871	759.4	873.4	1.150	1184.8	1143	5.21	5.02	1544	.2583
3	17	1	D_1	G	.924	.989	.0034	72.12	8.49	2399	.3485	836	791.7	.947	958.7	969.7	4.65	4.70	1562	.2888
3		2	F_1	G	.888	.981	.0037	66.27	8.14	2399	.3561	854.3	898.5	1.052	923	940.8	4.47	4.56	1576	.2900
4	18	1	N	F_1	.837	.873	.0043	57.03	7.55	2676	.3689	987.2	889.1	.901	870.3	996.5	3.78	4.33	1628	.2643
4	19	1	X	D_1	.928	.953	.0044	55.73	7.46	2676	.3703	990.9	—	—	943.1	989.6	4.10	4.30	1957	.2898
4		2	X	F_1	.937	.994	.0049	50.04	7.07	2676	.3791	1014.5	925.5	.912	947.2	952.8	4.12	4.14	2198	.3071
5	20	1	F_1	F_1	.867	1.060	.0046	67.90	8.24	2821	.2750	775.8	863.9	1.114	905.4	854	3.73	3.52	1885	.2390

CONFIDENTIAL

TABLE II.- Concluded

(g) 645 Plan Form

Model	Run	Point	Wing panel behavior		M_e	V_e/V_R	ρ_e, $\frac{\text{slugs}}{\text{cu ft}}$	μ_e	$\sqrt{\mu_e}$	ω_α, $\frac{\text{radians}}{\text{sec}}$	ω_R/ω_α	ω_R, $\frac{\text{radians}}{\text{sec}}$	ω_e, $\frac{\text{radians}}{\text{sec}}$	ω_e/ω_R	V_e, ft/sec	V_R, ft/sec	$\frac{V_e}{b_r\omega_\alpha}$	$\frac{V_R}{b_r\omega_\alpha}$	q_e, lb/ft^2	$\frac{V_e}{b_s\omega_\alpha\sqrt{\mu_e}}$
			Left	Right																
(Ref. 2)	1	1	D_1	G	1.361	1.271	0.0028	62.41	7.90	3179	0.3538	1125	—	—	1242.3	977.2	4.15	3.27	2161	0.3895
"		2	F_1	G	1.321	1.351	.0035	50.45	7.10	3179	.3659	1163	1313	1.129	1215.5	899.5	4.06	3.01	2586	.4240
"	2	1	D_1	G	.964	.899	.0024	73.69	8.59	3179	.3436	1092	—	—	939.9	1045.9	3.14	3.50	1060	.2710
"		2	F_1	G	1.081	.969	.0023	76.90	8.78	3179	.3405	1082	1138	1.052	1033.4	1066.8	3.45	3.57	1228	.2915
"		3	E_1	G	1.233	1.070	.0023	78.19	8.84	3179	.3398	1080	—	—	1144.7	1069.8	3.82	3.58	1507	.3207
"		4	D_2	G	1.316	1.250	.0029	59.98	7.74	3179	.3562	1132	—	—	1202.6	962.2	4.02	3.22	2097	.3848
"		5	F_2	G	1.311	1.320	.0034	51.63	7.19	3179	.3646	1159	1319	1.138	1199	908.4	4.00	3.04	2444	.4130
"	3	1	F_1	G	1.055	.985	.0024	72.52	8.52	3179	.3445	1095	942	.860	1021.7	1036.9	3.41	3.47	1253	.2970
"	4	1	F_1	G	1.153	.938	.0018	98.25	9.92	3179	—	—	1401	—	1106.9	1180.4	3.70	3.95	1103	.2764
"		2	E_1	G	1.270	.964	.0016	110.53	10.51	3179	—	—	—	—	1195.1	1240.1	3.99	4.15	1143	.2816
"		3	D_2	G	1.356	1.285	.0030	58.86	7.67	3179	.3573	1136	—	—	1228.5	956.2	4.10	3.20	2264	.3967
"		4	F_2	G	1.354	1.272	.0035	51.19	7.65	3179	.3576	1137	1376	1.210	1216.7	956	4.06	3.19	2591	.3939
"	5	1	D_1	N	1.315	1.333	.0035	50.30	7.09	3179	.3661	1164	—	—	1199.1	899.5	4.00	3.01	2516	.4189
"		2	F_1	N	1.316	1.367	.0038	46.70	6.83	3179	.3701	1176	1382	1.175	1193	872.6	3.98	2.92	2704	.4326
"	6	1	D_1	N	1.320	1.301	.0033	53.13	7.29	3179	.3631	1154	—	—	1197.6	920.4	4.00	3.08	2366	.4069
"		2	F_1	N	1.308	1.308	.0035	51.24	7.16	3179	.3650	1160	1414	1.219	1184	905.4	3.95	3.03	2453	.4096
"	7	1	F_1	F_1	1.041	.974	.0025	70.33	8.39	3179	.3466	1102	942	.855	1001.3	1028	3.34	3.44	1253	.2956
"	8	1	F_1	F_1	1.055	.987	.0024	74.79	8.65	3179	.3426	1089	1005	.923	1037.8	1051.9	3.47	3.52	1292	.2972
"		2	E_1	E_1	1.205	1.086	.0023	76.40	8.74	3179	.3412	1085	—	—	1152.2	1060.8	3.85	3.55	1527	.3265
"		3	D_2	D_2	1.279	1.202	.0027	66.09	8.13	3179	.3504	1114	—	—	1202.9	1001.1	4.02	3.35	1953	.3665
"		4	F_2	F_2	1.277	1.248	.0030	58.94	7.68	3179	.3572	1136	1238	1.090	1193.2	956.2	3.98	3.20	2136	.3848
"	9	1	F_1	F_1	1.034	.983	.0026	68.90	8.30	3179	.3578	1137	961	.845	1001.3	1019	3.34	3.41	1303	.2988
"	10	1	F_1	F_1	1.078	.982	.0023	77.44	8.80	3179	.3402	1081	1074	.994	1047.5	1066.8	3.50	3.57	1262	.2948
"		2	E_1	E_1	1.220	1.068	.0022	79.46	8.91	3179	—	—	—	—	1152.5	1078.8	3.85	3.61	1461	.3204
"	11	1	F_1	F_1	1.103	.974	.0022	79.74	8.93	3179	—	—	1382	—	1054.2	1081.8	3.52	3.62	1222	.2924
"	12	1	F_1	F_1	.981	.985	.0028	62.85	7.93	3179	.3534	1123	1049	.934	955.7	980.1	3.19	3.28	1279	.2985
"	13	1	F_1	F_1	.877	.941	.0033	54.14	7.36	3179	.3620	1151	967	.840	868.6	923.4	2.90	3.09	1245	.2923
"	14	1	F_1	F_1	.832	.935	.0037	48.39	6.96	3179	.3681	1170	1023	.874	827.3	884.5	2.76	2.96	1266	.2944
"	15	1	D_1	D_1	.773	.917	.0042	42.11	6.50	3179	.3751	1192	—	—	769.9	839.7	2.57	2.81	1243	.2934
"		2	F_1	F_1	.763	.917	.0043	41.13	6.42	3179	.3763	1196	1047	.875	761.5	830.7	2.54	2.78	1247	.2938
"	16	1	D_1	D_1	.848	.925	.0034	52.47	7.24	3179	.3638	1156	—	—	845.9	914.4	2.82	3.06	1216	.2894
"		2	F_1	F_1	.891	.981	.0035	50.30	7.09	3179	.3661	1164	1062	.912	982.1	899.5	2.95	3.01	1362	.3431
"	17	1	F_1	F_1	1.040	.979	.0026	69.33	8.33	3179	.3474	1104	1018	.922	1003.3	1025	3.35	3.43	1308	.2983
"	18	1	F_1	X_1	1.014	1.005	.0030	59.55	7.72	3179	.3566	1134	1049	.925	967.4	962.2	3.23	3.22	1404	.3104

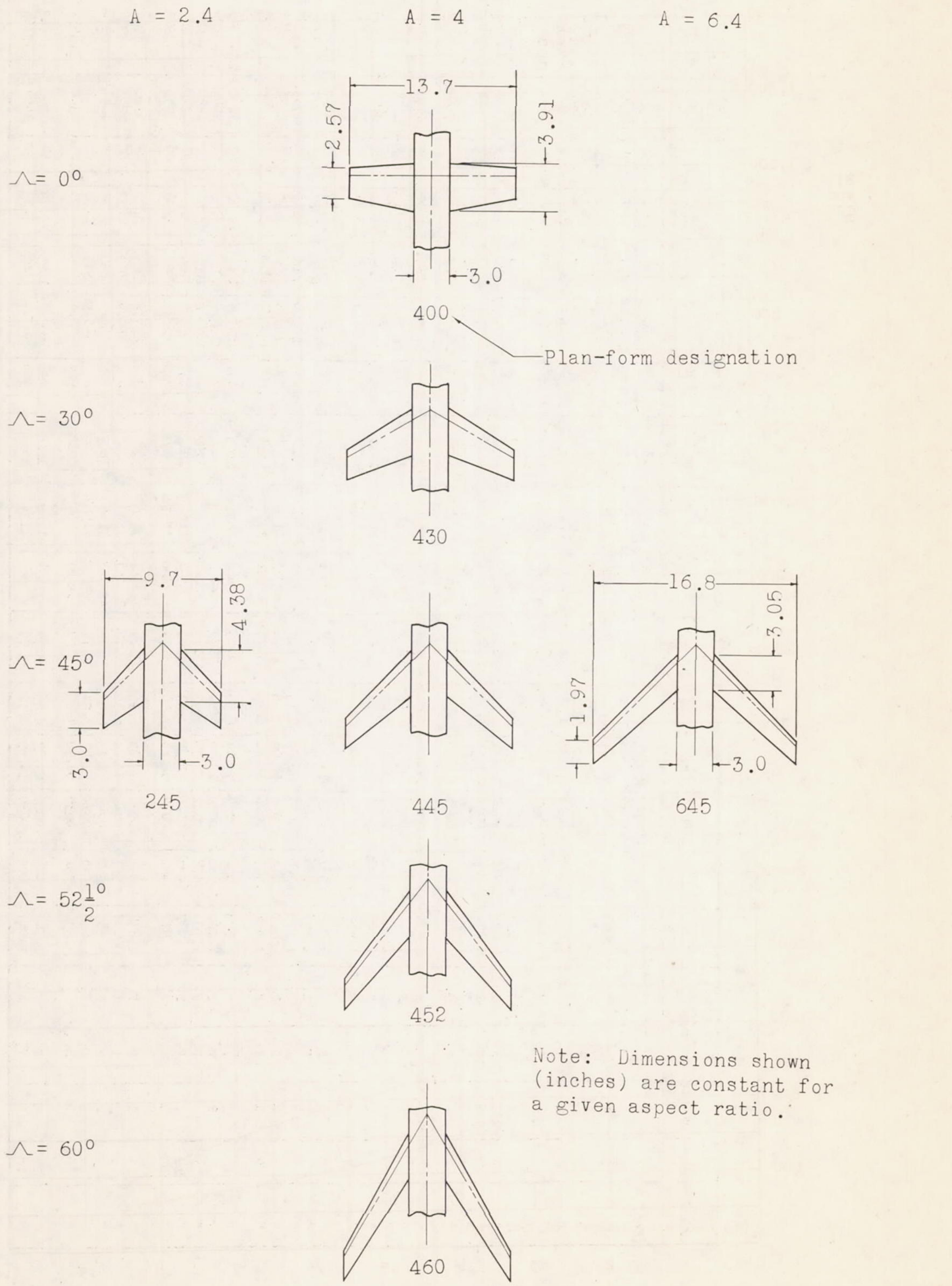

Figure 1.- Plan forms of flutter models giving aspect ratio, sweep angle, plan-form dimensions, and model designations.

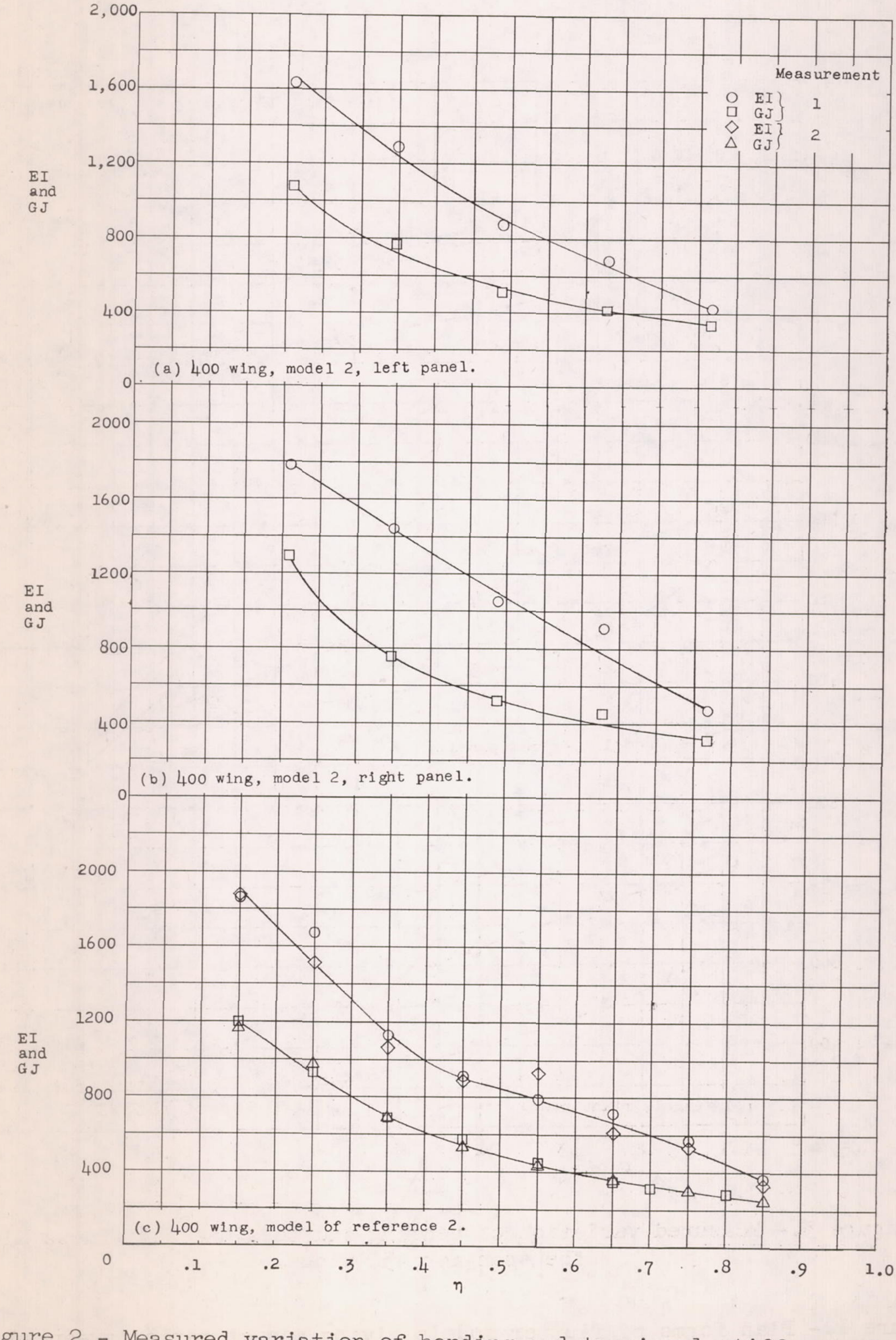

Figure 2.- Measured variation of bending and torsional stiffness along the span for 400 wings.

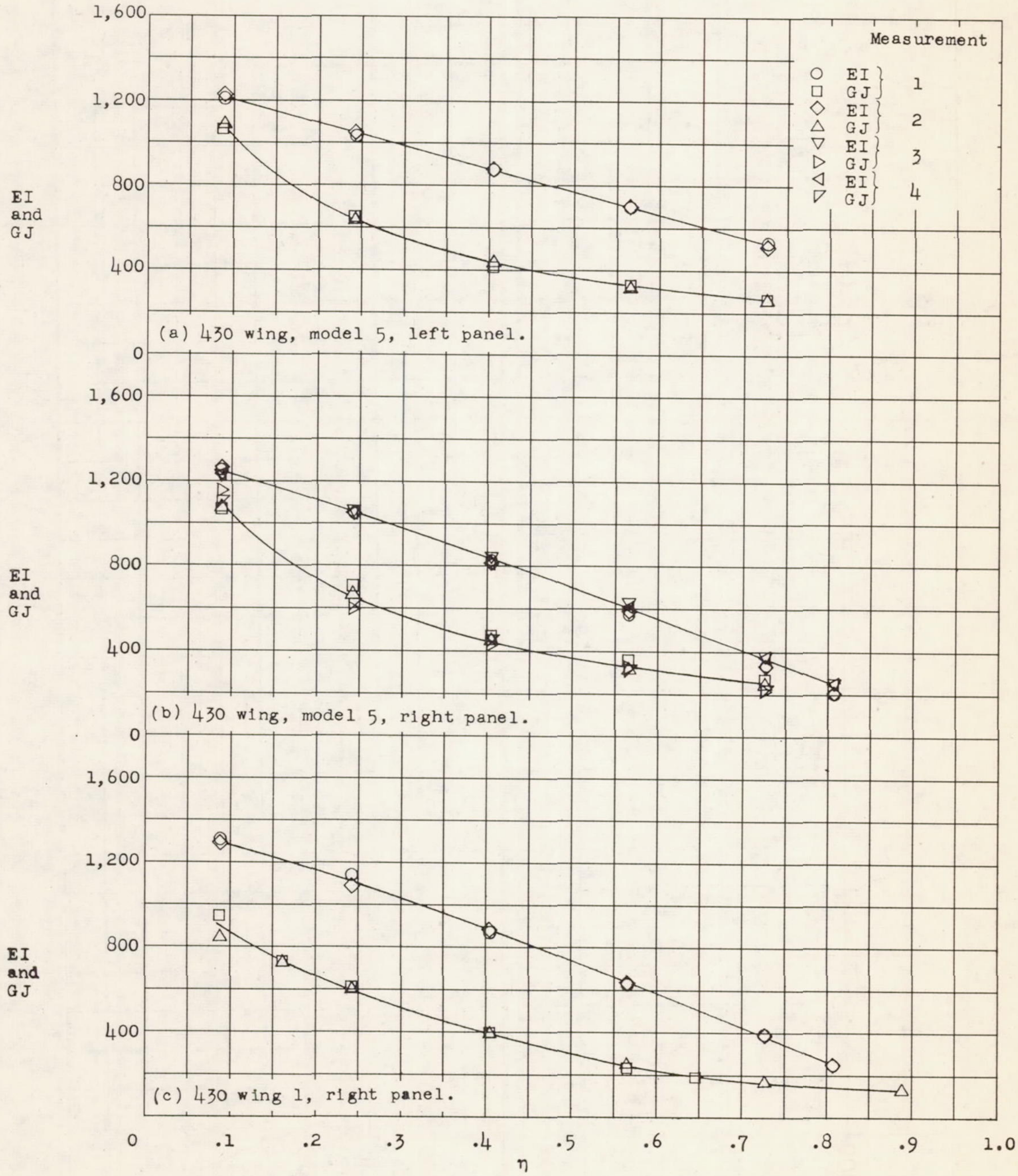

Figure 3.- Measured variation of bending and torsional stiffness along the span for 430 wings.

CONFIDENTIAL

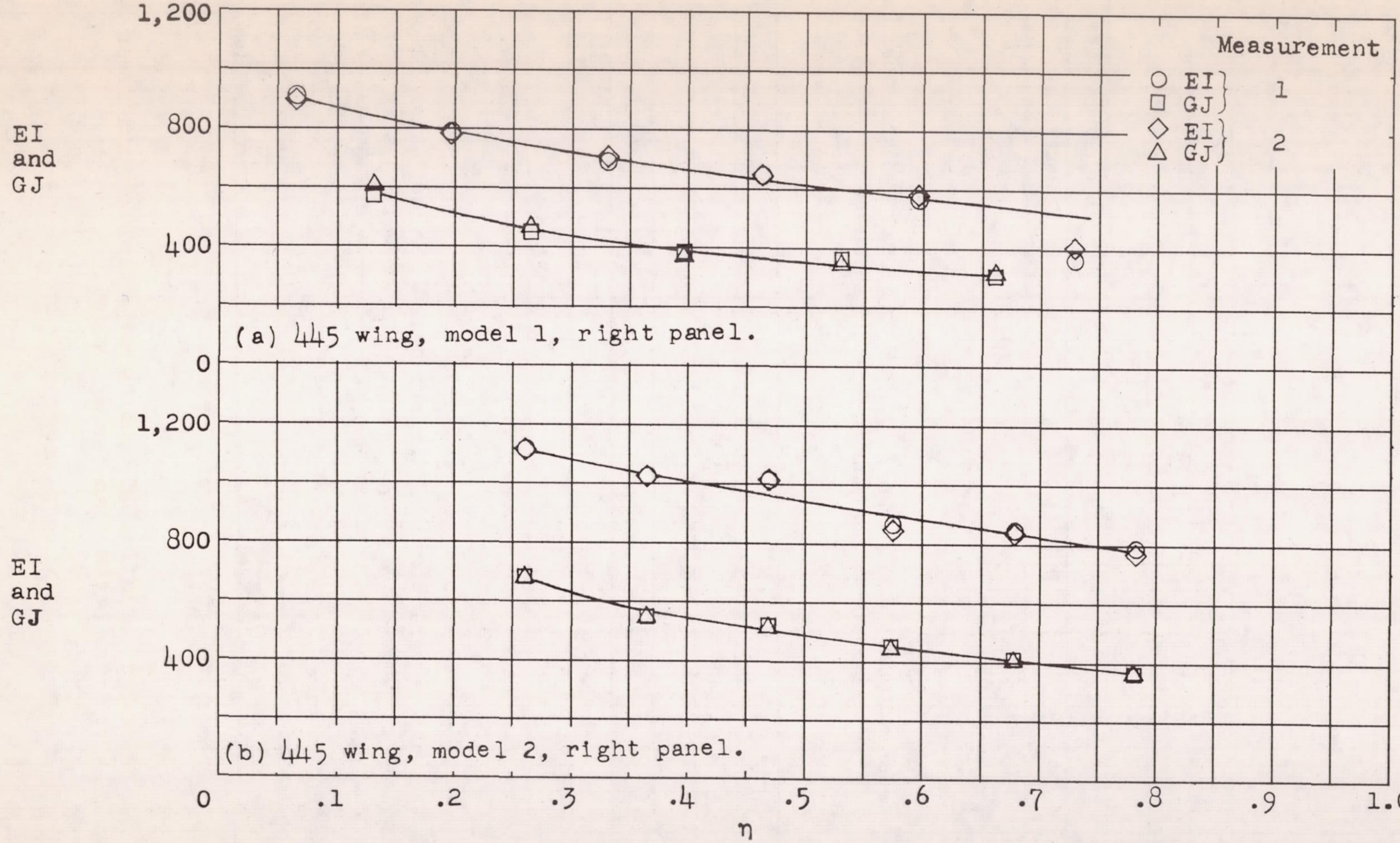

Figure 4.- Measured variation of bending and torsional stiffness along the span for 445 wings.

CONFIDENTIAL

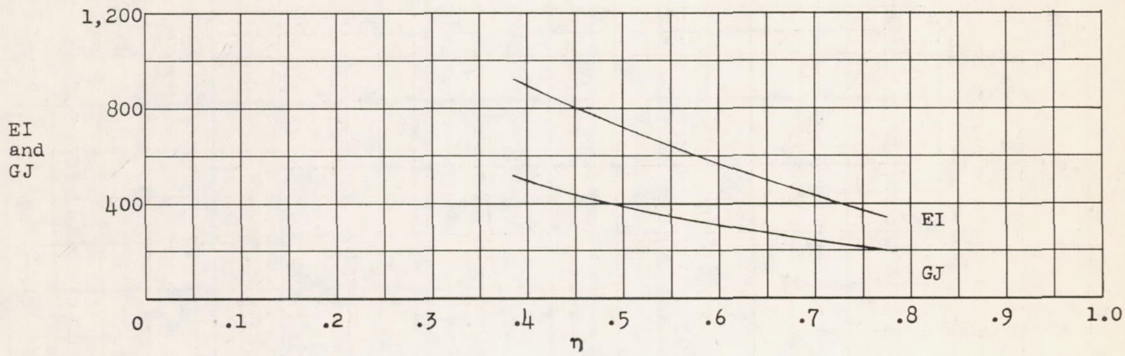

Figure 5.- Measured variation of bending and torsional stiffness along the span for 452 wing (model of ref. 2).

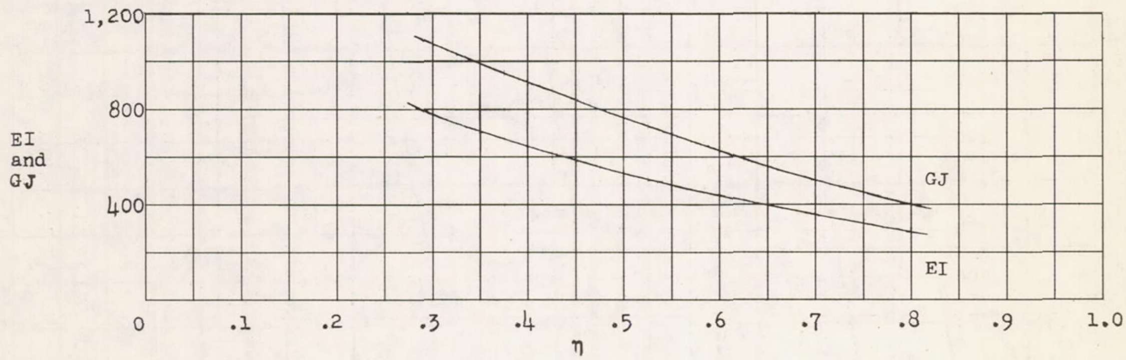

Figure 6.- Spanwise variations of the estimated bending and torsional stiffnesses of the 645 magnesium wing. Values were scaled from the measured variation on a similar wing of 2017-T aluminum alloy (formerly designated 17S-T) as follows: $(EI)_{mag} = (EI)_{al} \times \frac{E_{mag}}{E_{al}}$ and $(GJ)_{mag} = (GJ)_{al} \times \frac{G_{mag}}{G_{al}}$.

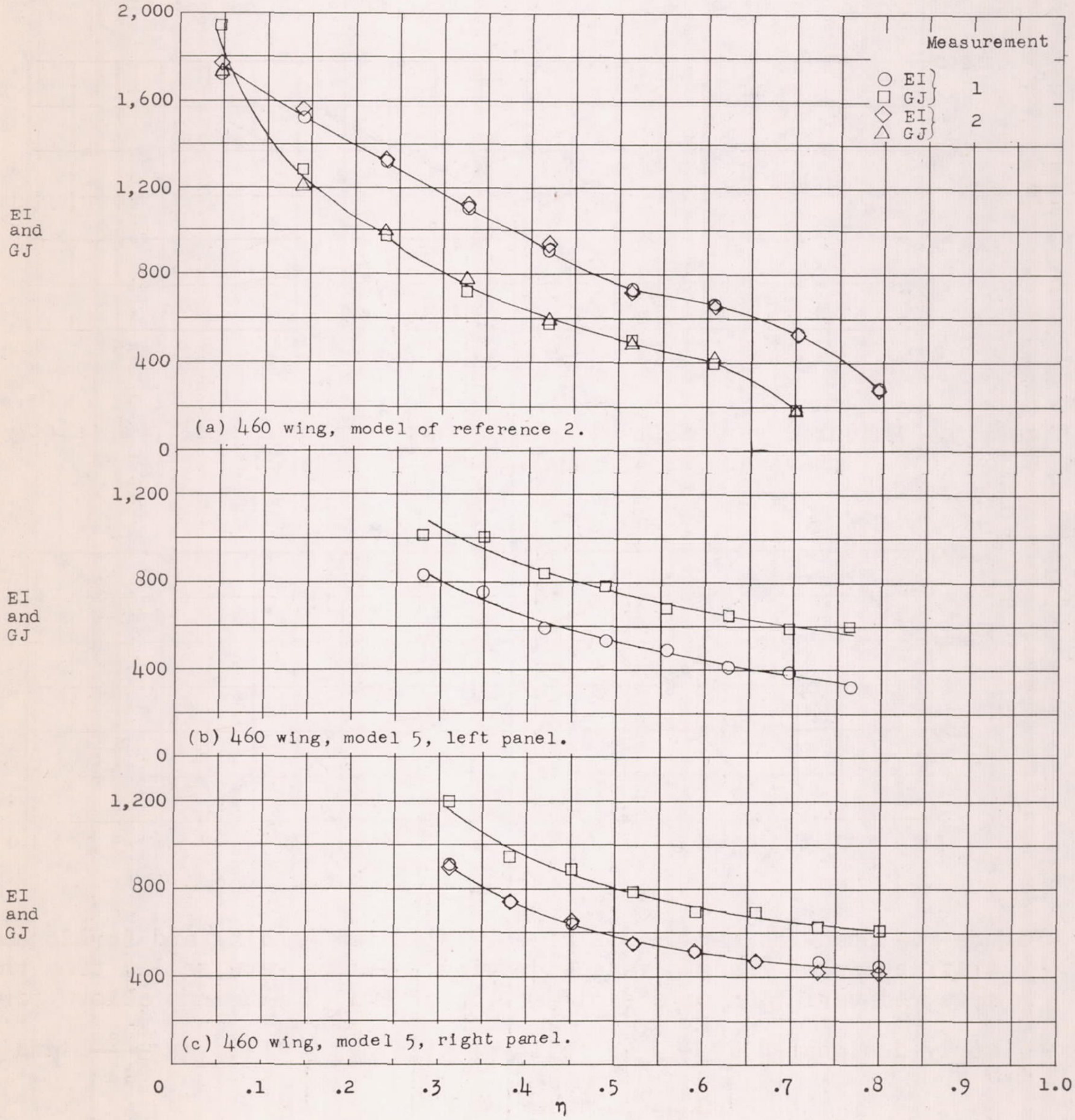

Figure 7.- Measured variation of bending and torsional stiffness along the span for 460 wings.

CONFIDENTIAL

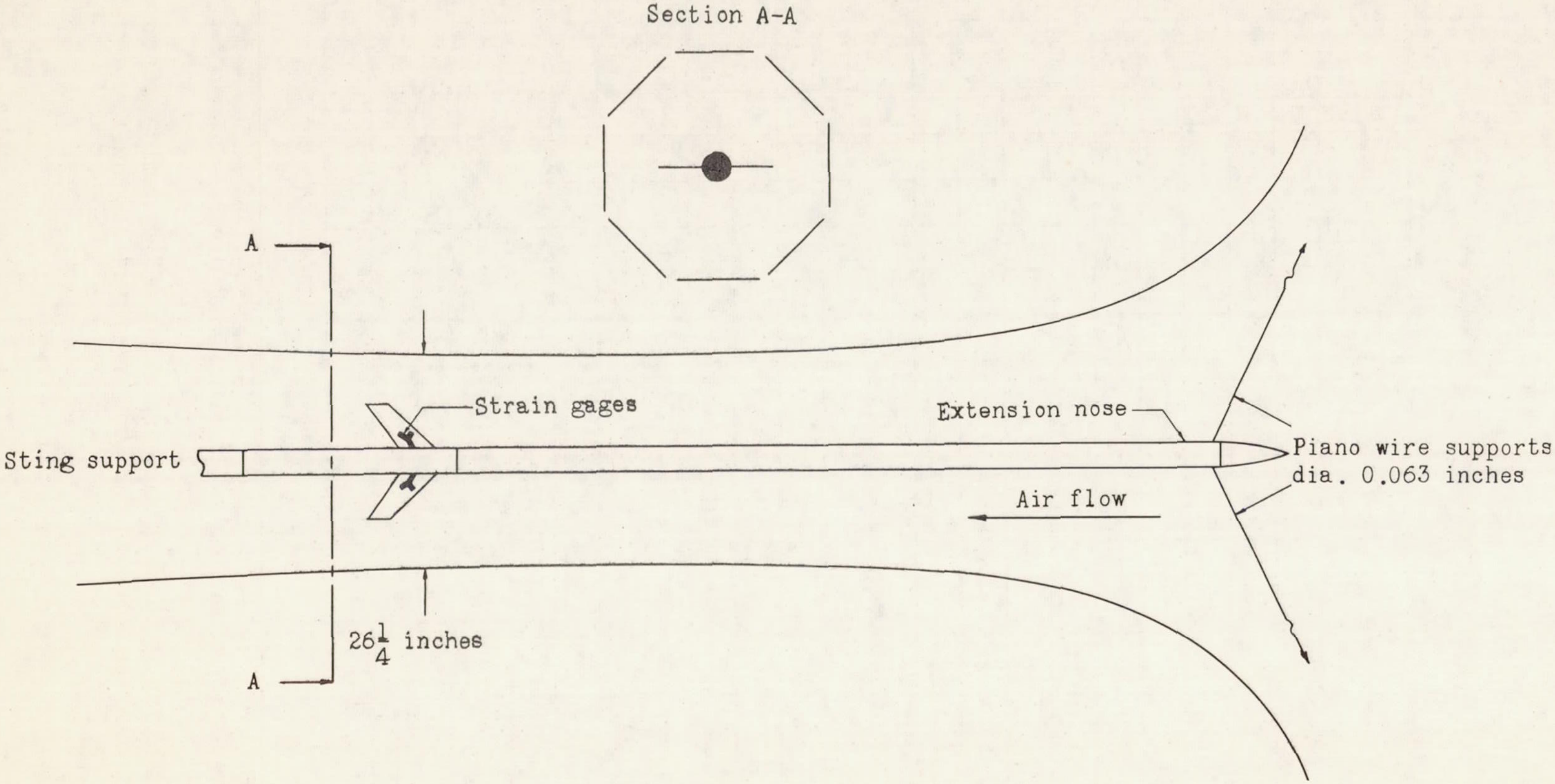

Figure 8.- Plan view of Langley transonic blowdown tunnel with flutter model installed.

CONFIDENTIAL

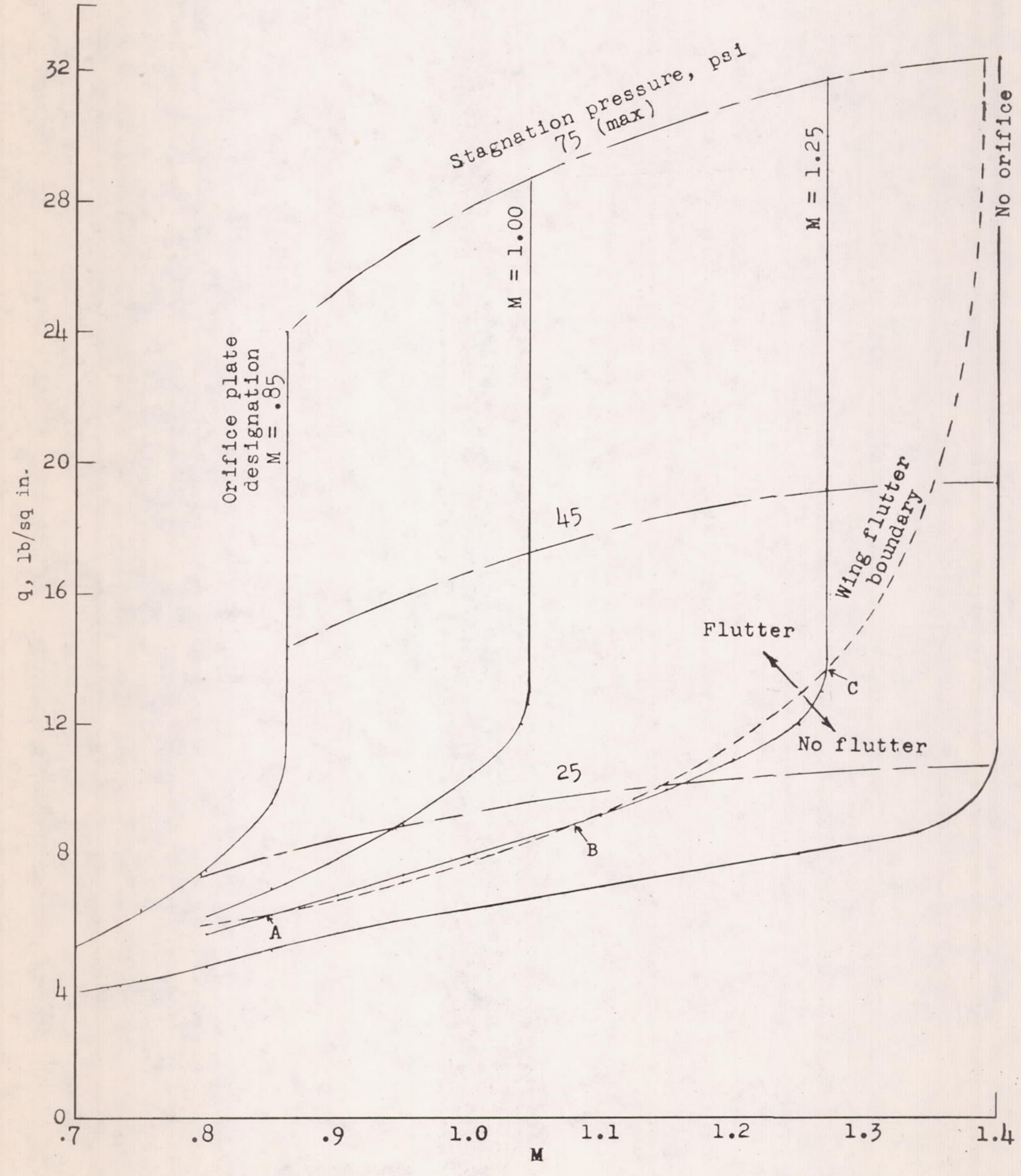

Figure 9.- Variation with Mach number of tunnel dynamic pressure curves for several orifice conditions, and an example wing-flutter-boundary curve.

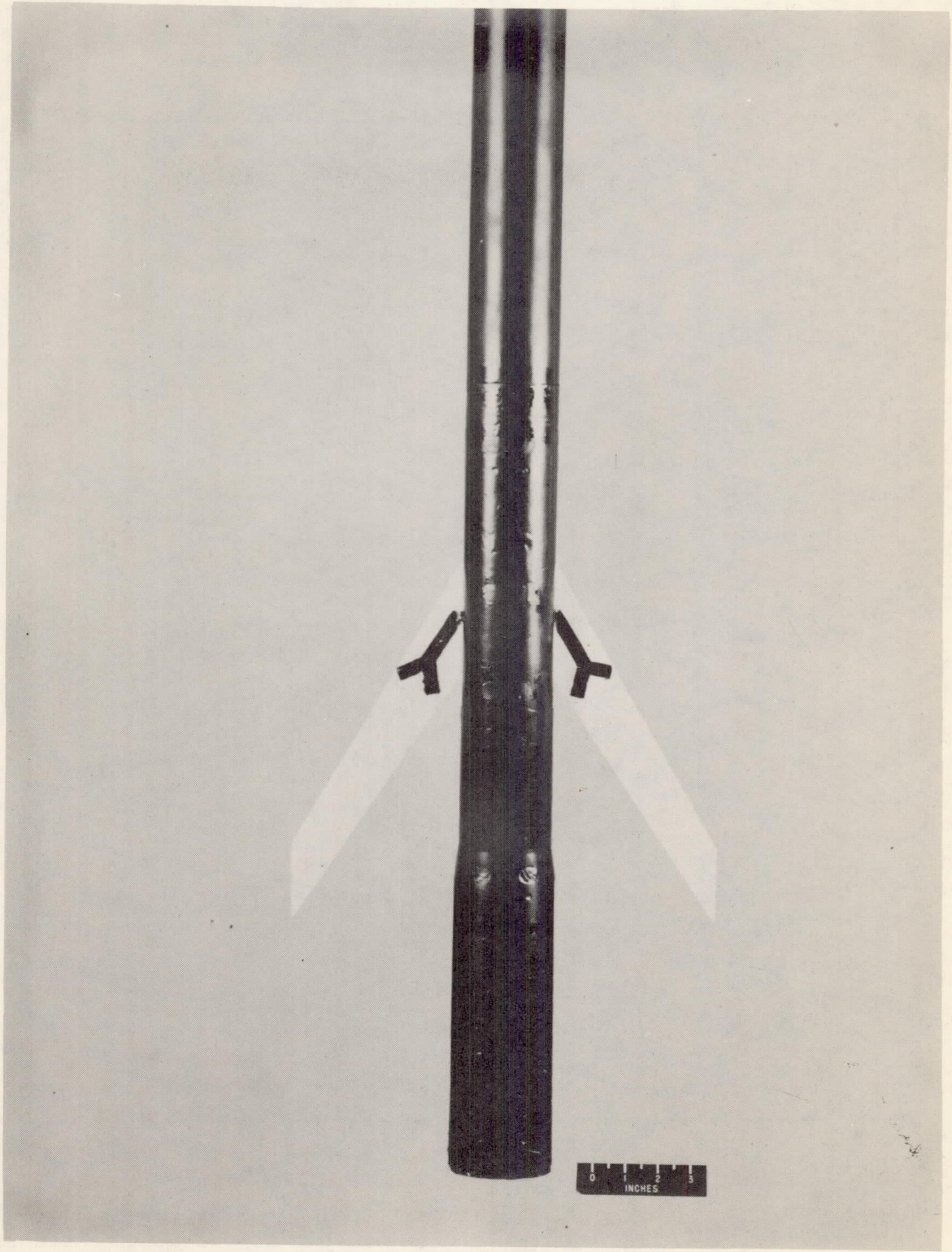

L-79715.1

Figure 10.- Example of flutter model mounted in sting fuselage.

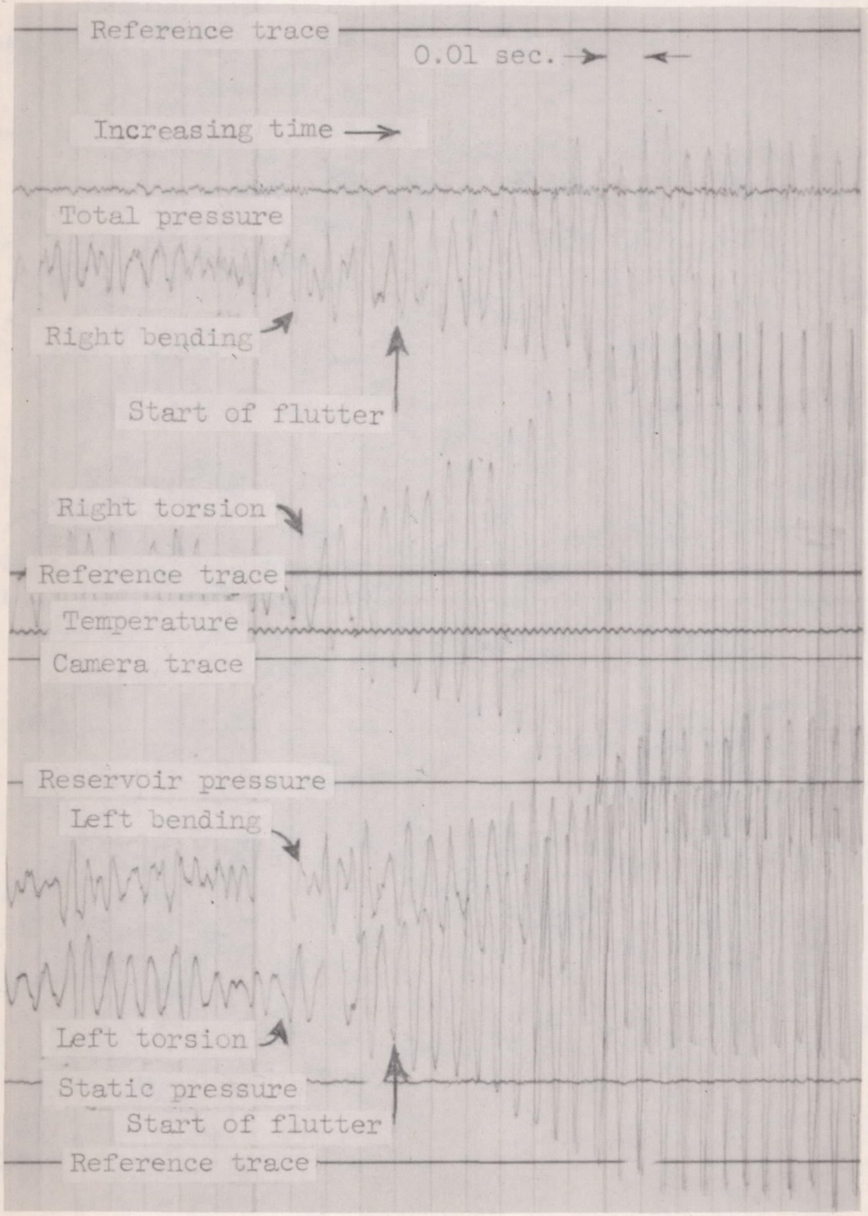

Figure 11.- Sample oscillograph record of flutter test (445 wing at M = 0.813).

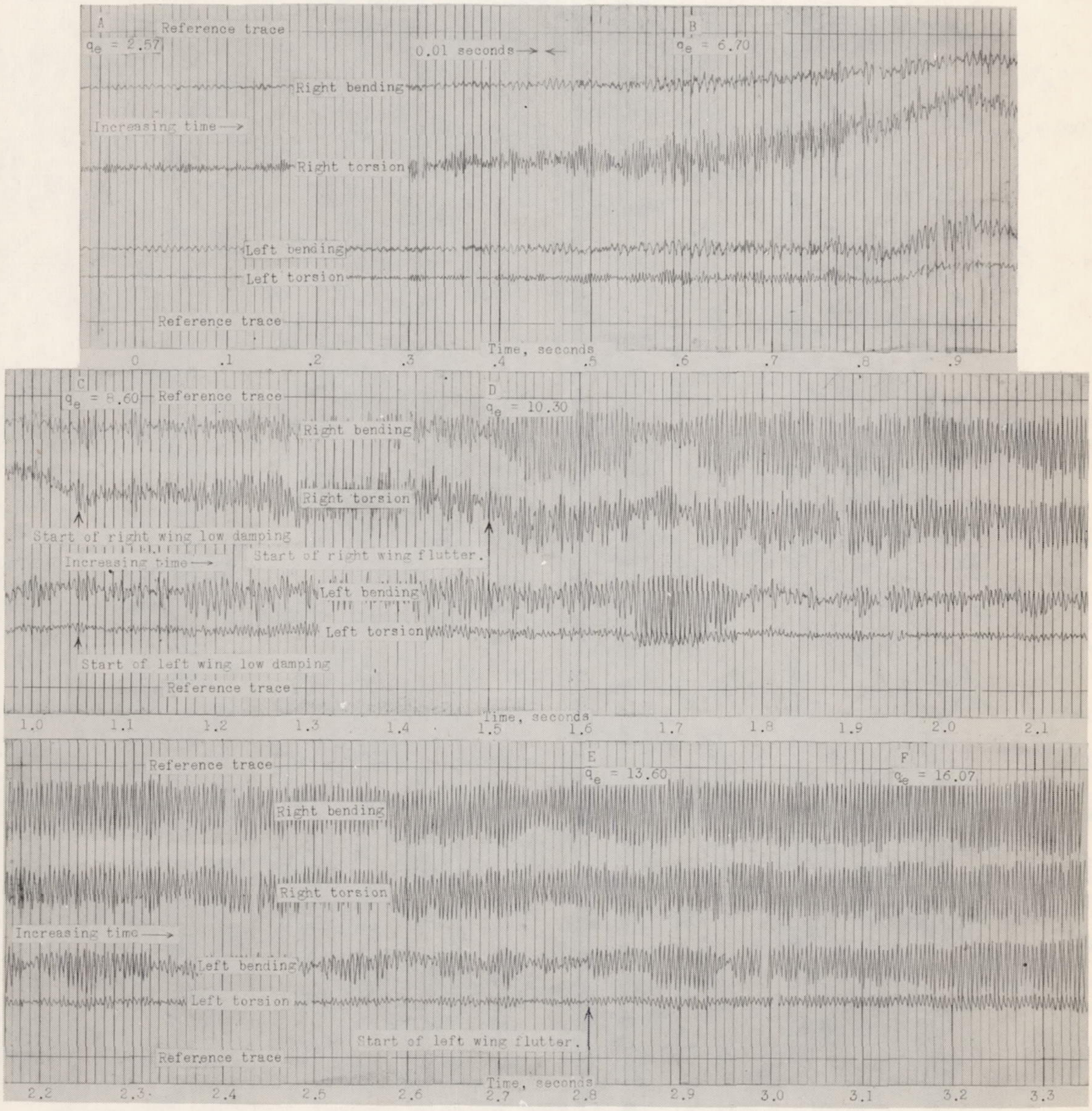

Figure 12.- Tracing of a section of an oscillograph record showing low damping and flutter which occurred on a 400 wing during a flutter test run.

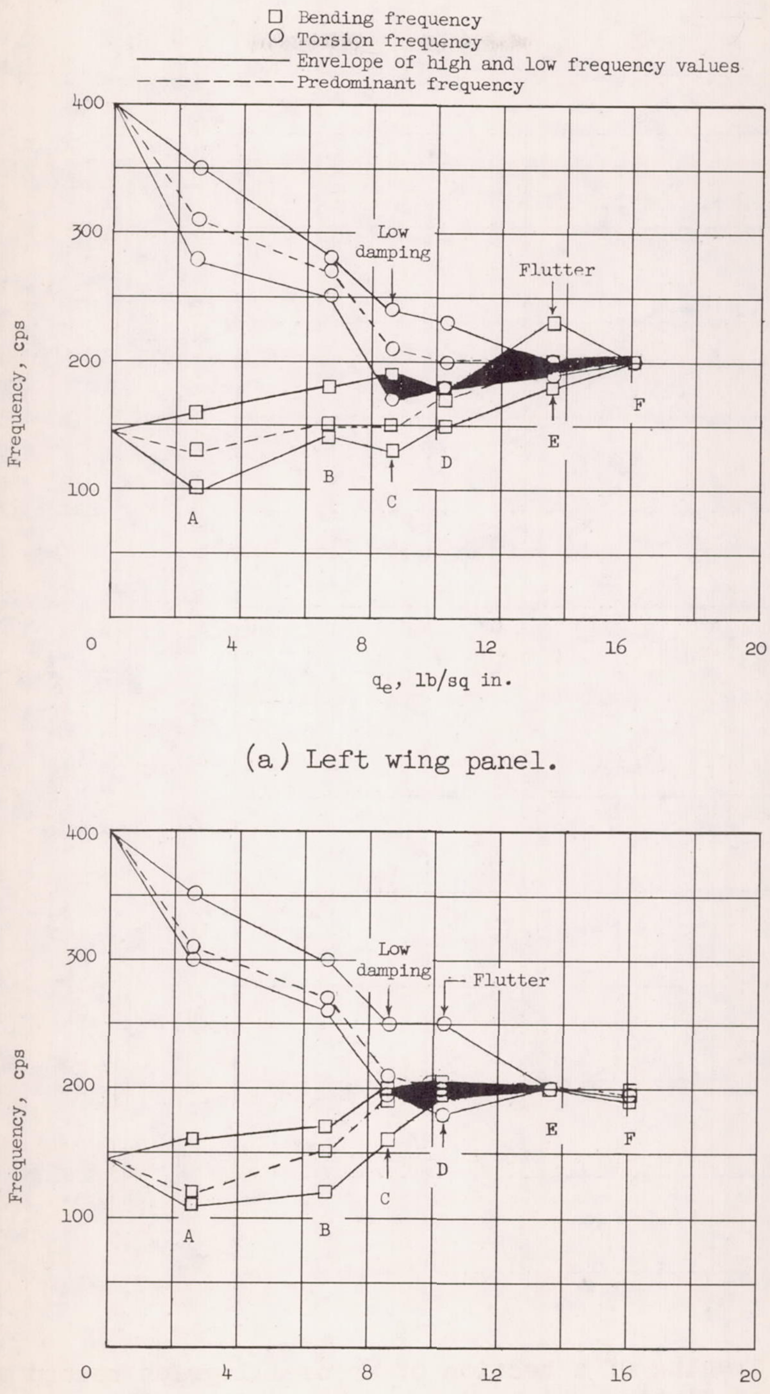

(a) Left wing panel.

(b) Right wing panel.

Figure 13.- Variation of bending and torsion frequencies of a 400 wing with dynamic pressure during a test run. Shaded areas indicate low damping region.

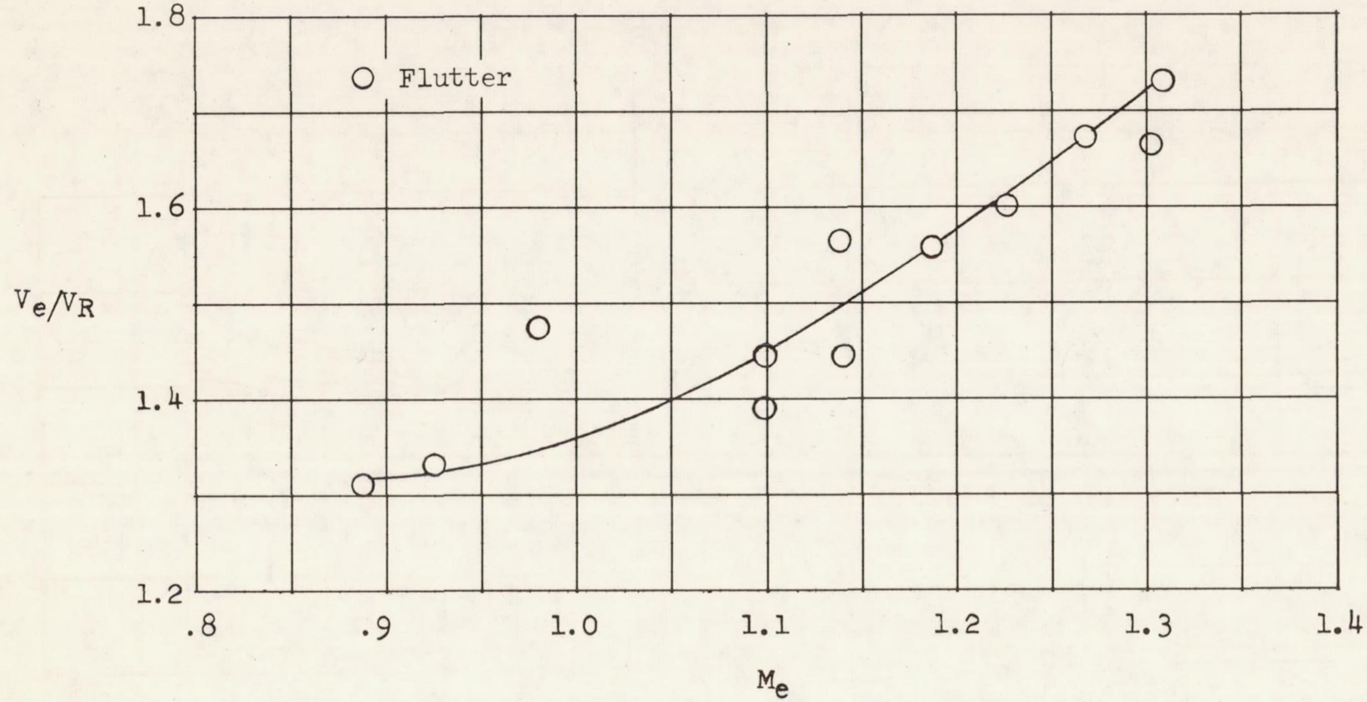

(a) 245 plan form.

Figure 14.- Variation of flutter-speed ratio with Mach number for the various flutter-model plan forms.

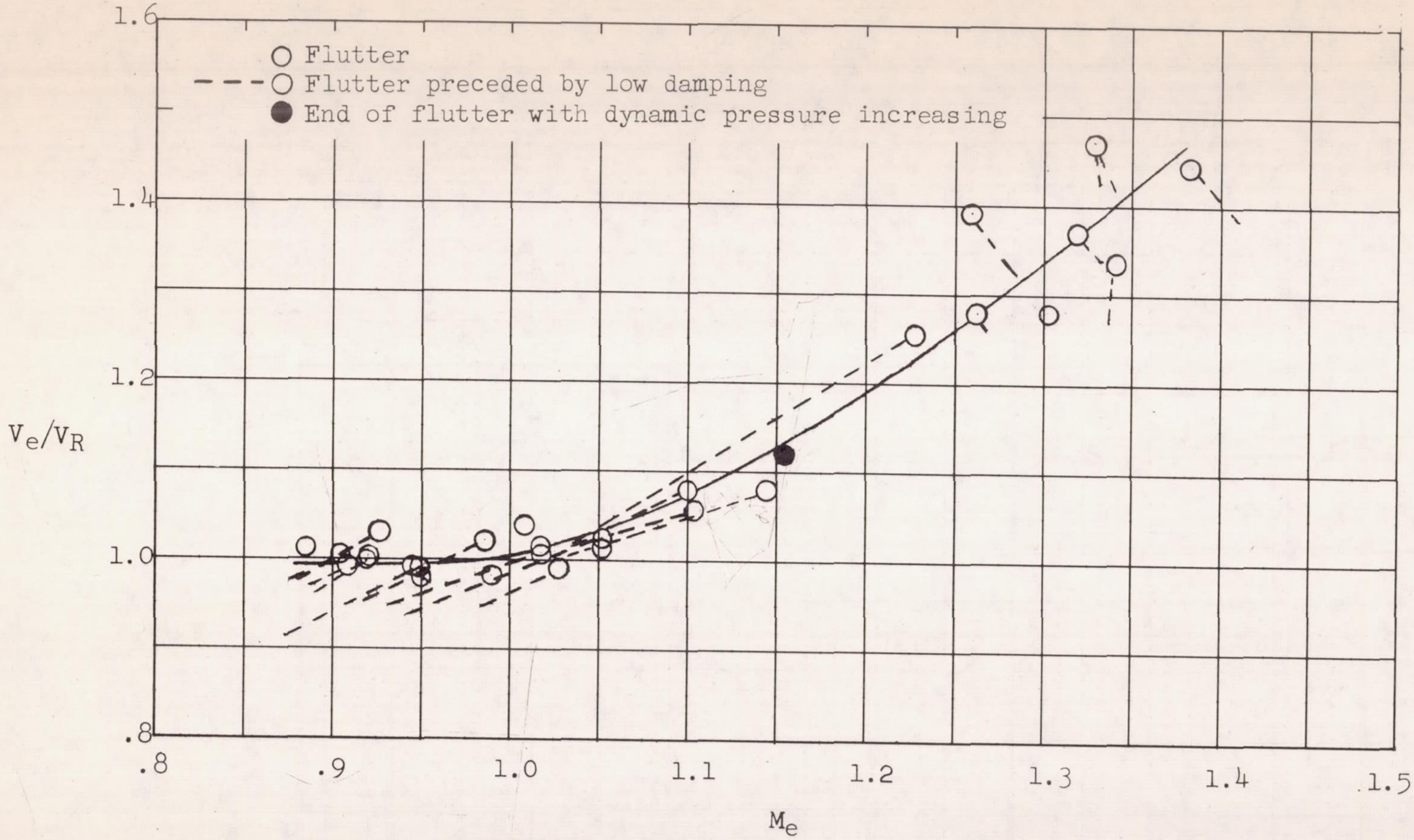

(b) 400 plan form.

Figure 14.- Continued.

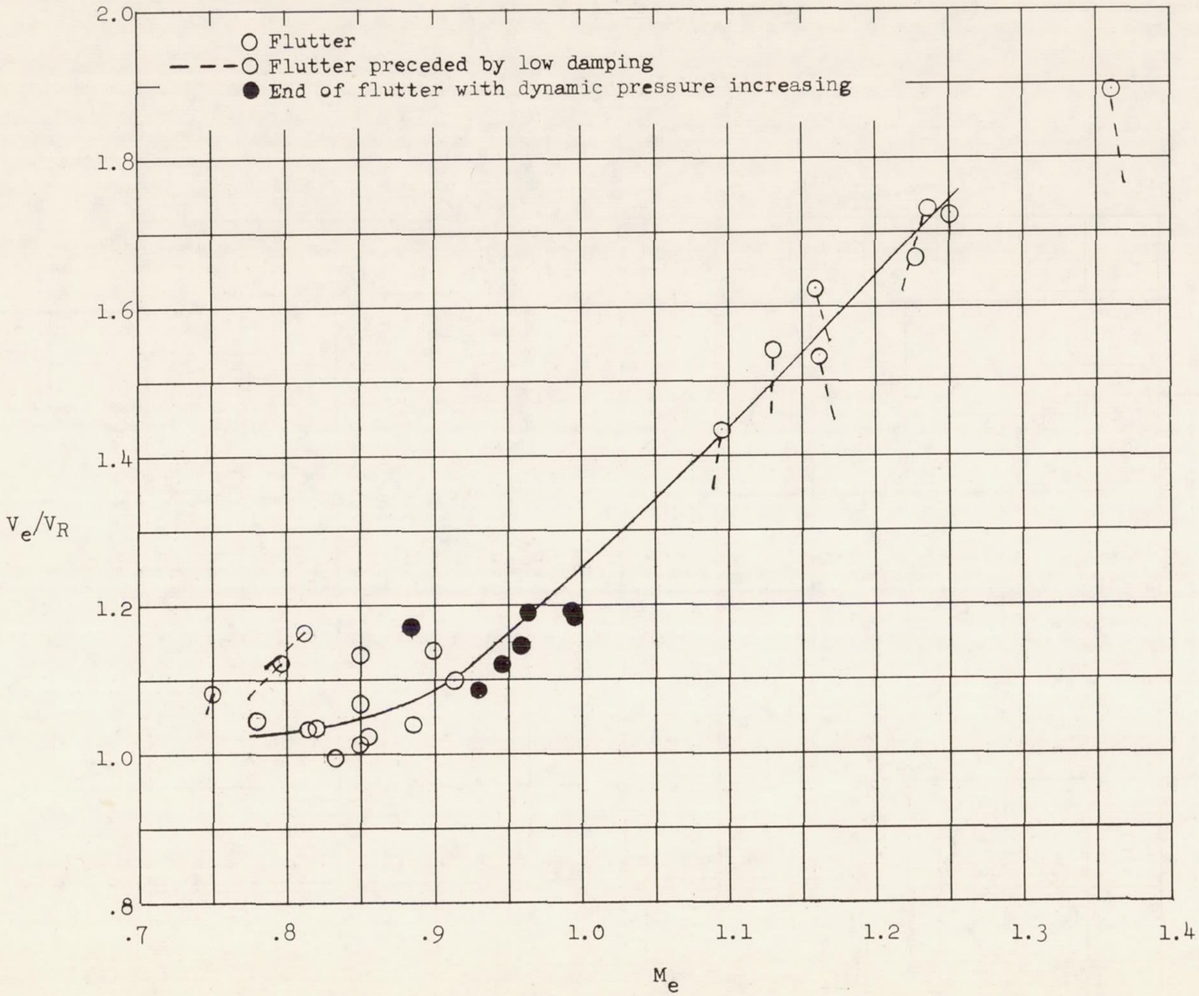

(c) 430 plan form.

Figure 14.- Continued.

CONFIDENTIAL

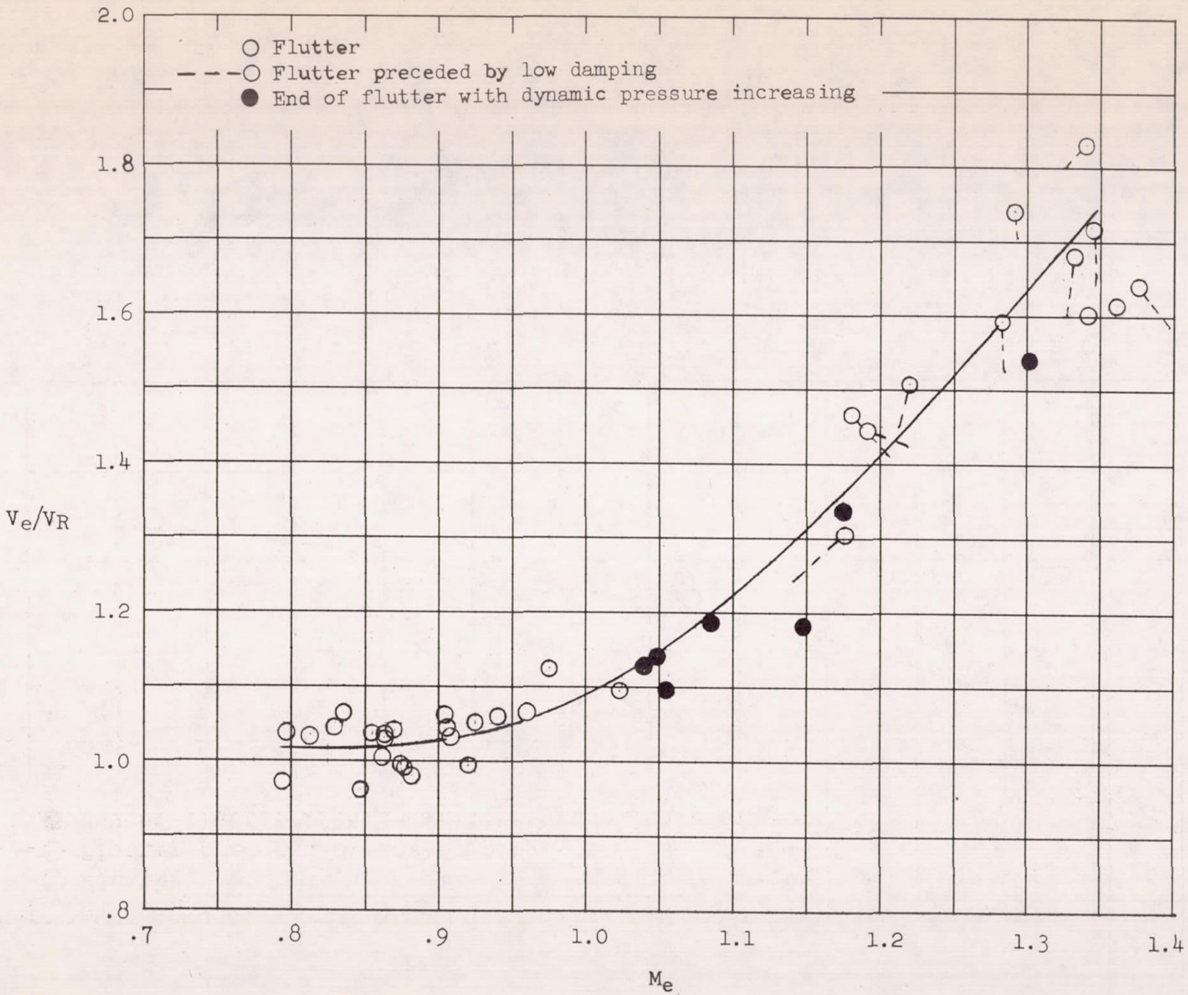

(d) 445 plan form.

Figure 14.- Continued.

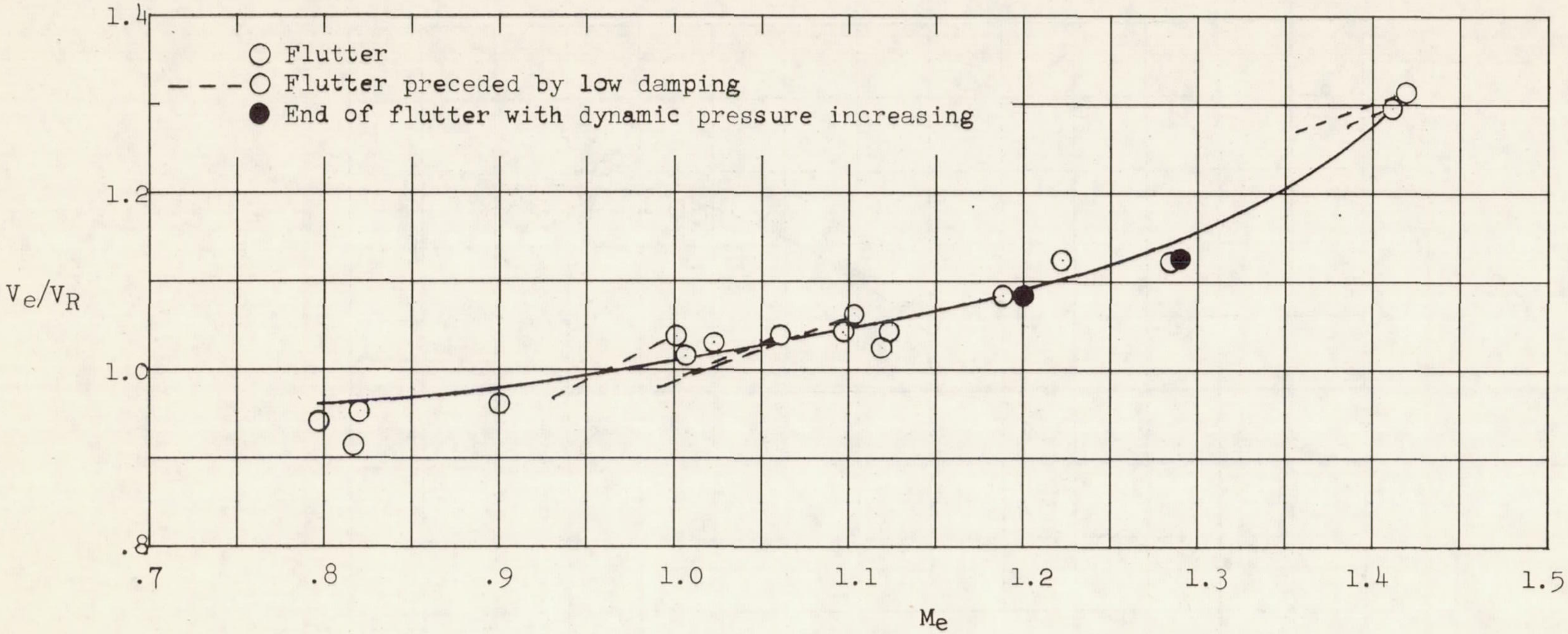

(e) 452 plan form.

Figure 14.- Continued.

CONFIDENTIAL

CONFIDENTIAL

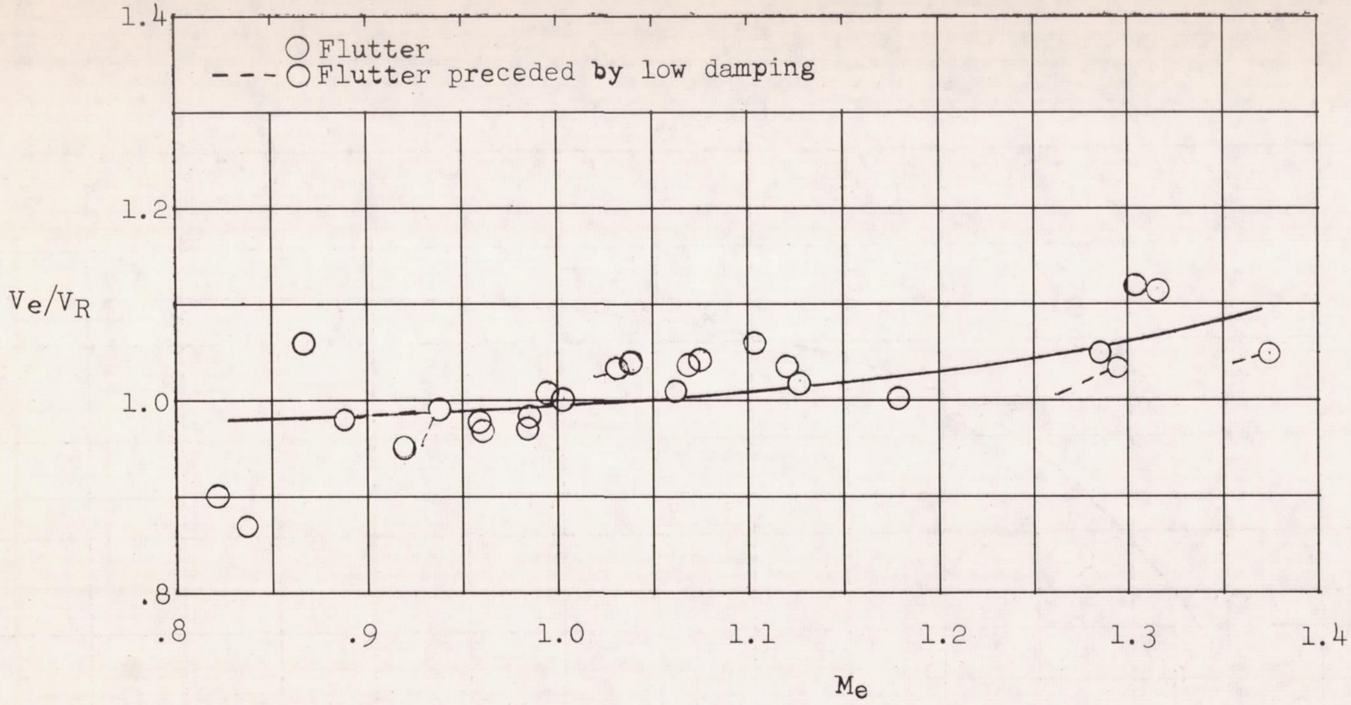

(f) 460 plan form.

Figure 14.- Continued.

CONFIDENTIAL

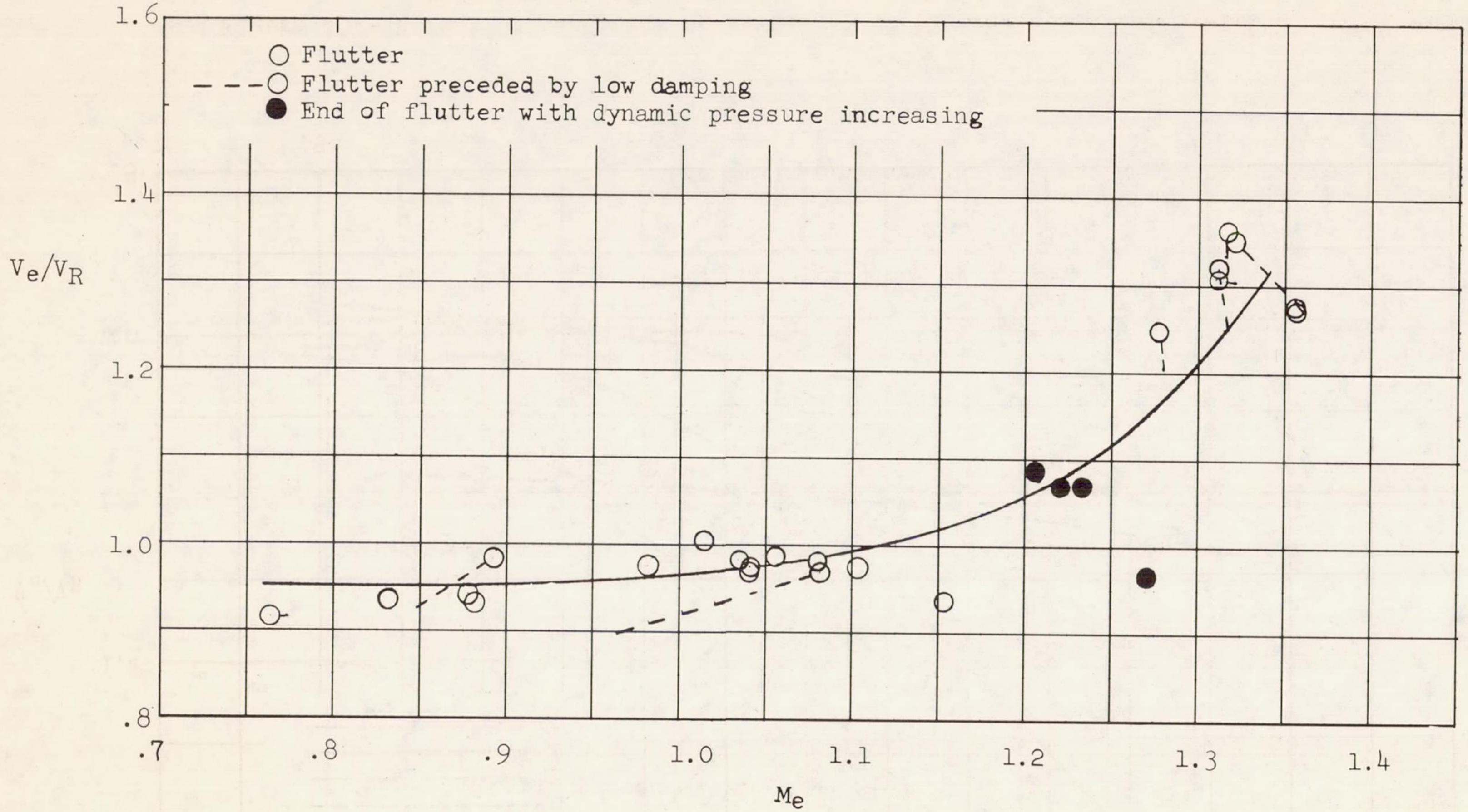

(g) 645 plan form.

Figure 14.- Concluded.

CONFIDENTIAL

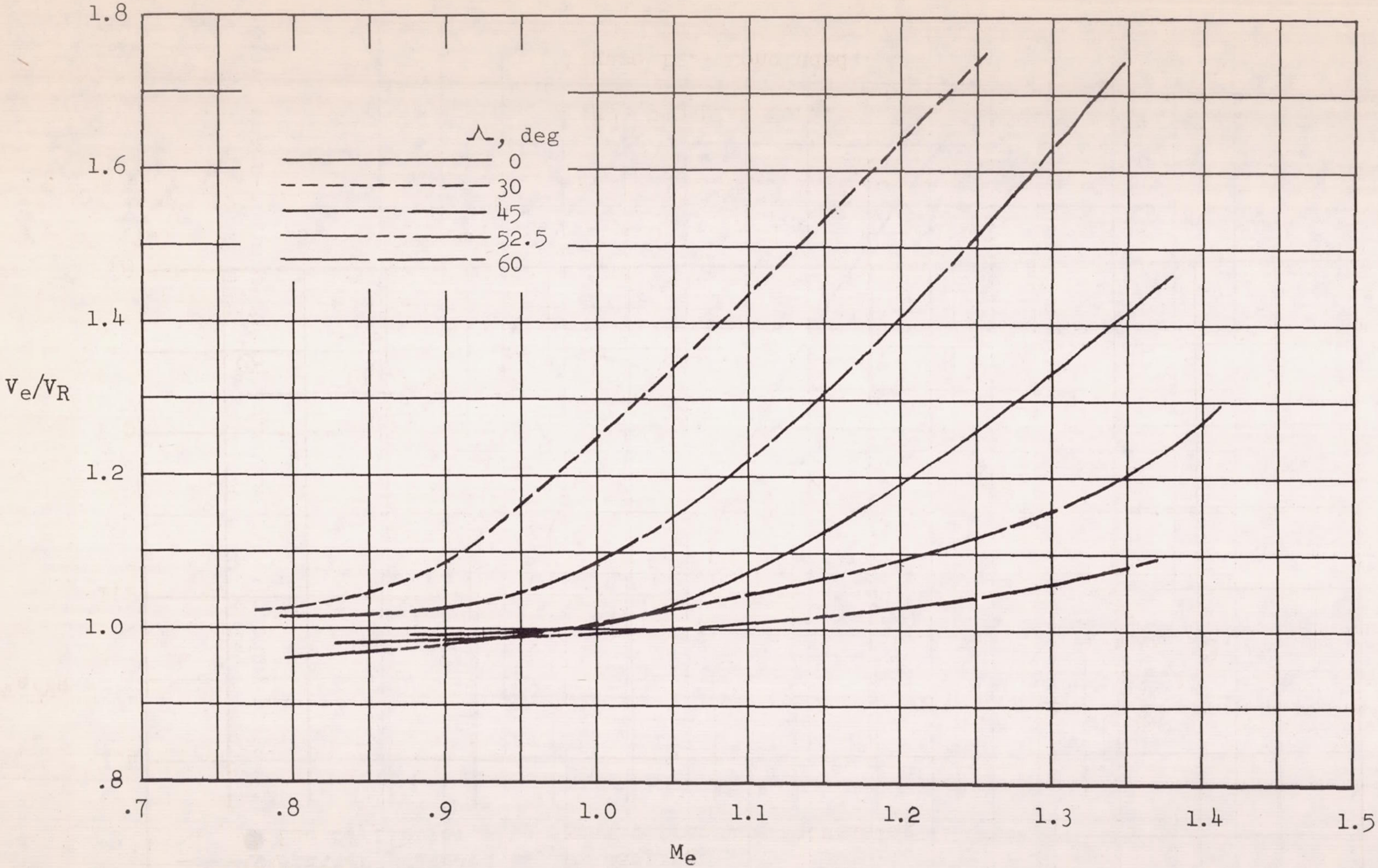

Figure 15.- Effect of sweepback on variation of flutter-speed ratio with Mach number for wings with aspect ratio 4.

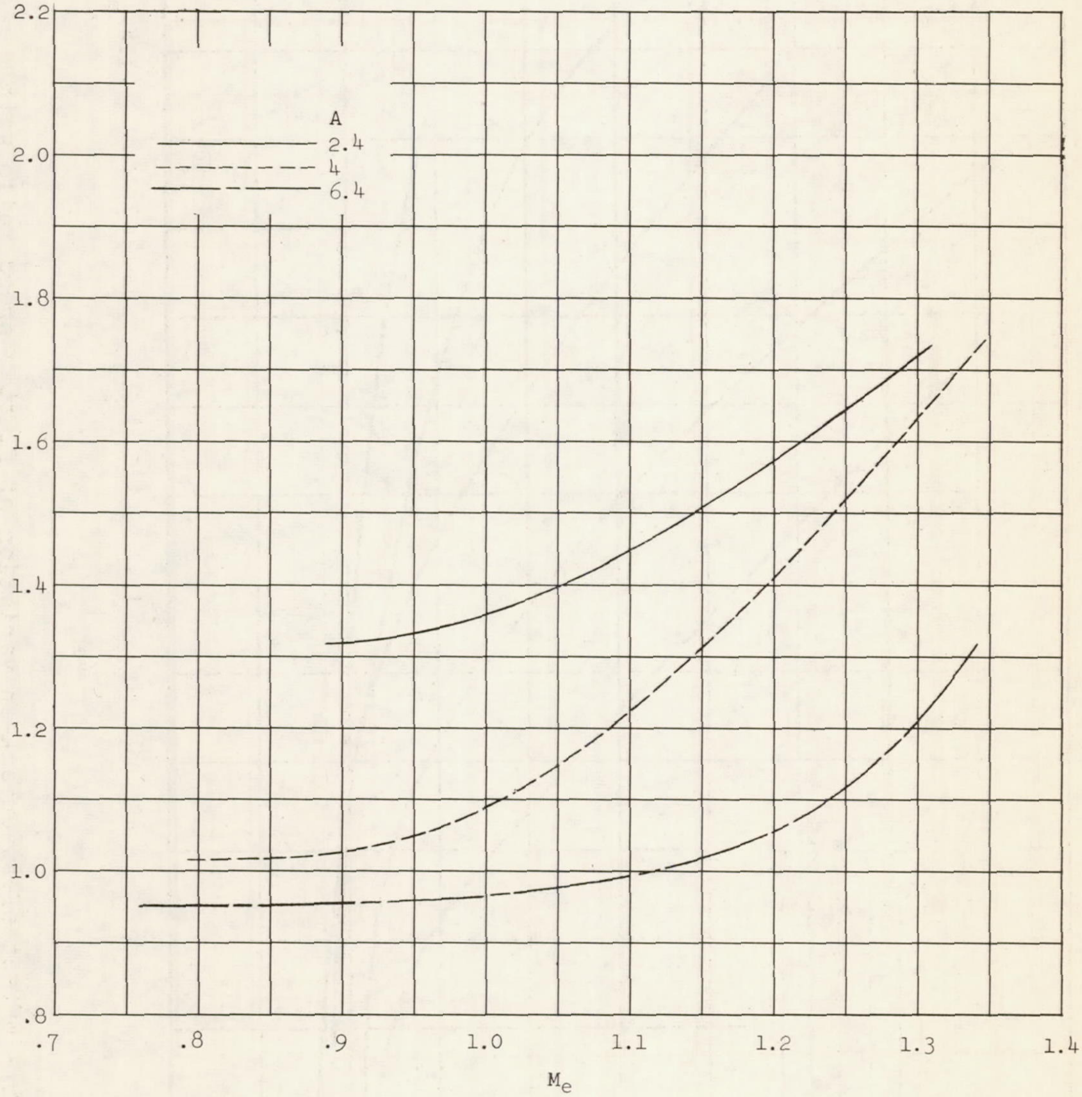

Figure 16.- Effect of aspect ratio on variation of flutter-speed ratio with Mach number for wings with 45° sweepback.

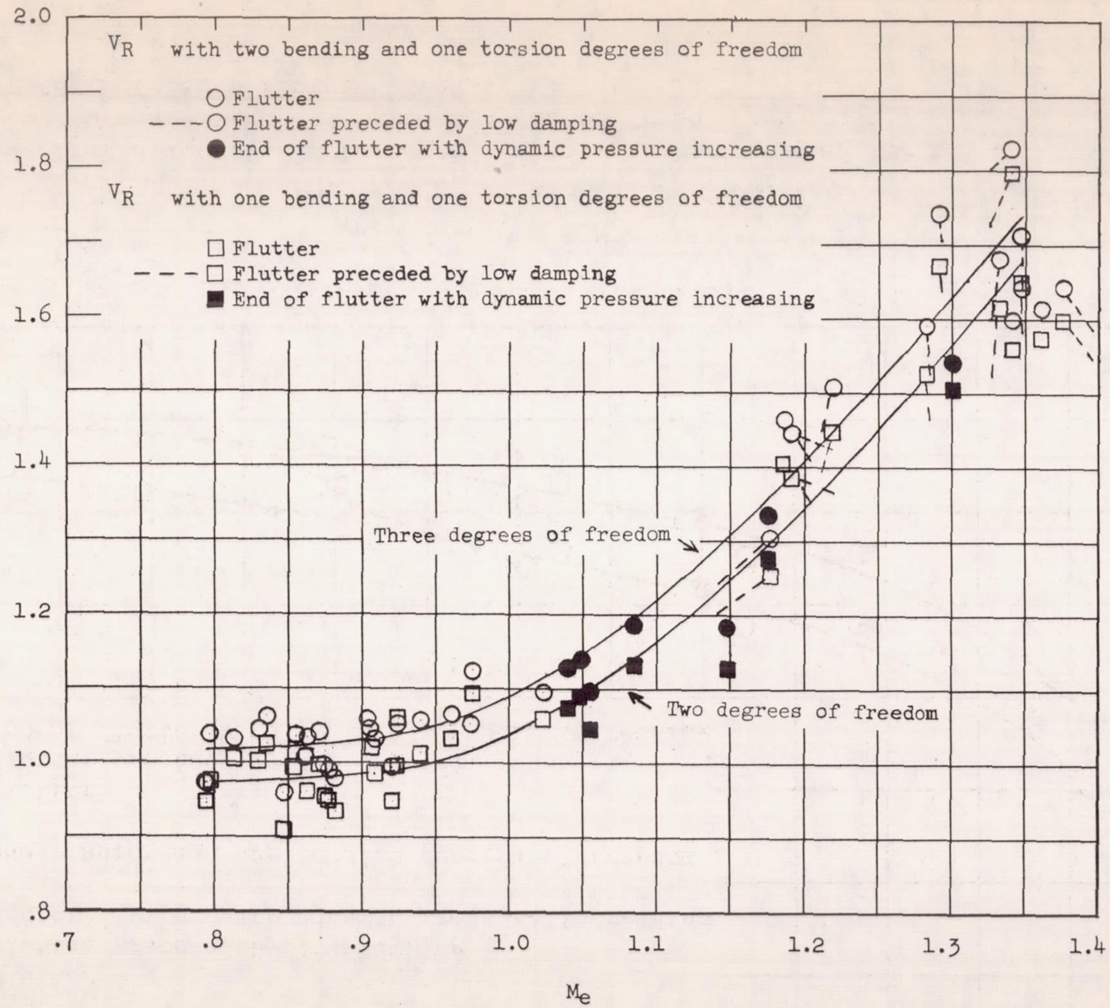

Figure 17.- Variation of flutter-speed ratio with Mach number for the 445 plan form when two and three degrees of freedom were used in computing the reference flutter speeds.

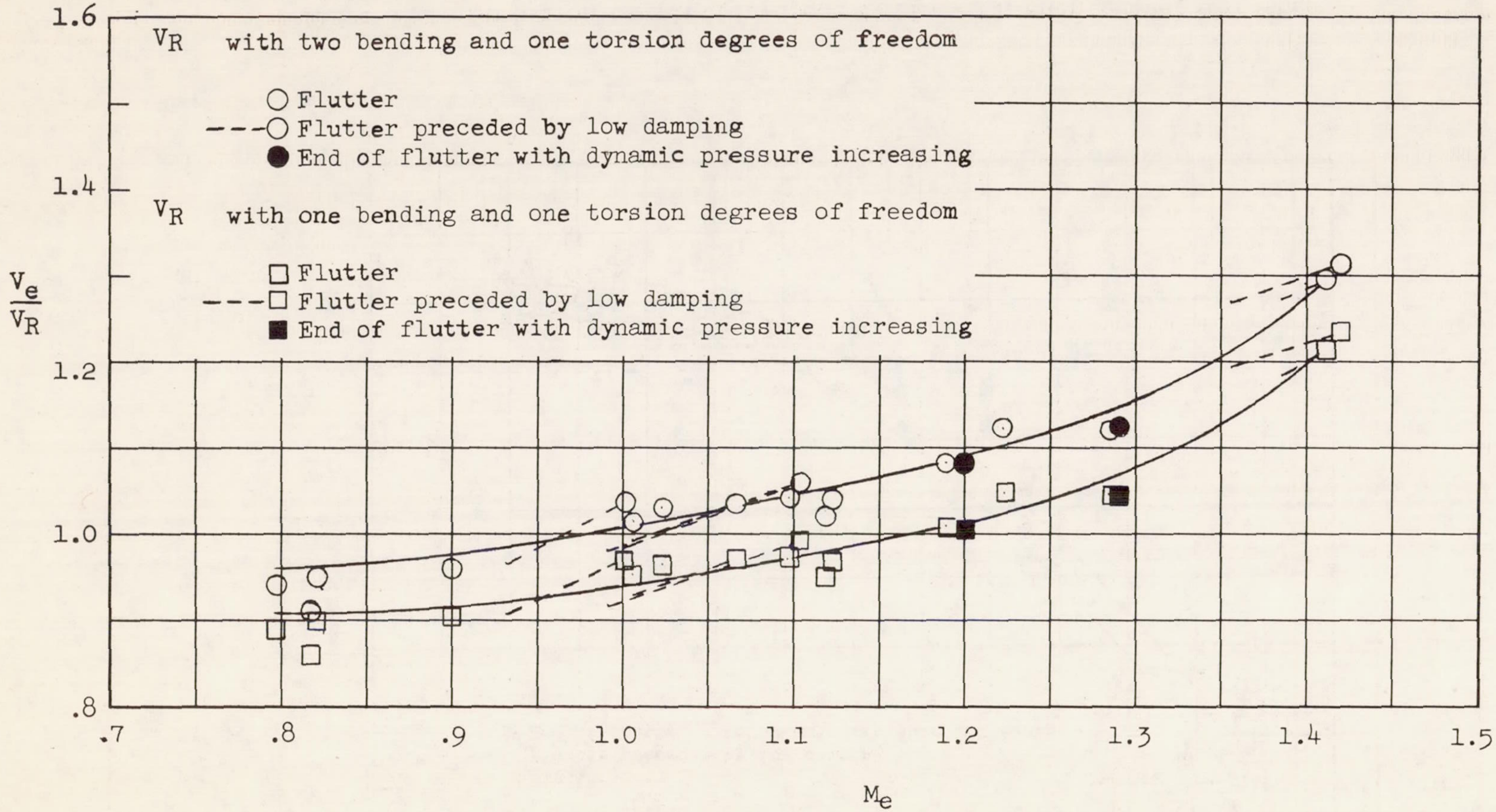

Figure 18.- Variation of flutter-speed ratio with Mach number for the 452 plan form when two and three degrees of freedom were used in computing the reference flutter speeds.

CONFIDENTIAL

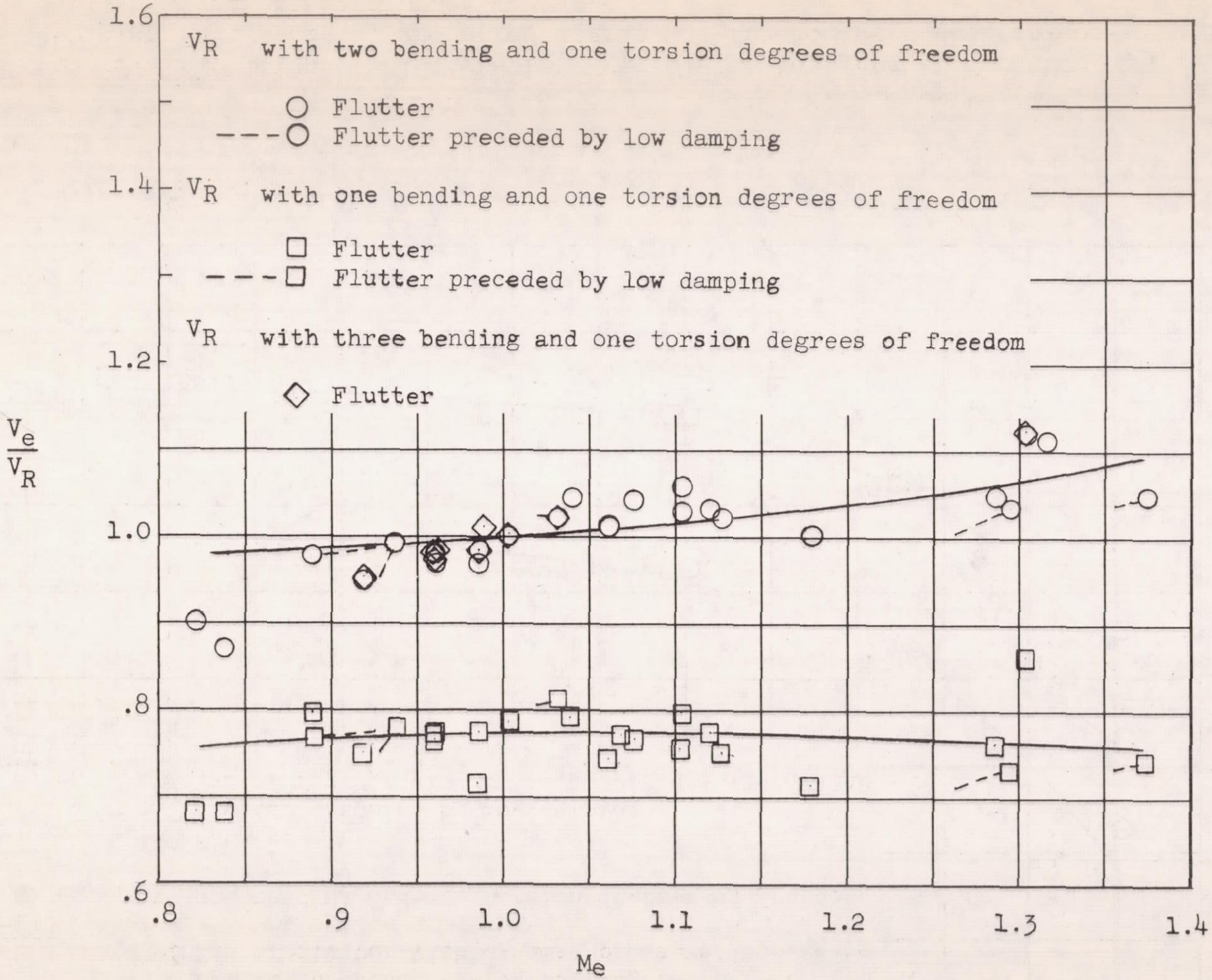

Figure 19.- Variation of flutter-speed ratio with Mach number for the 46° plan form when two, three, and four degrees of freedom were used in computing the reference flutter speeds.

CONFIDENTIAL

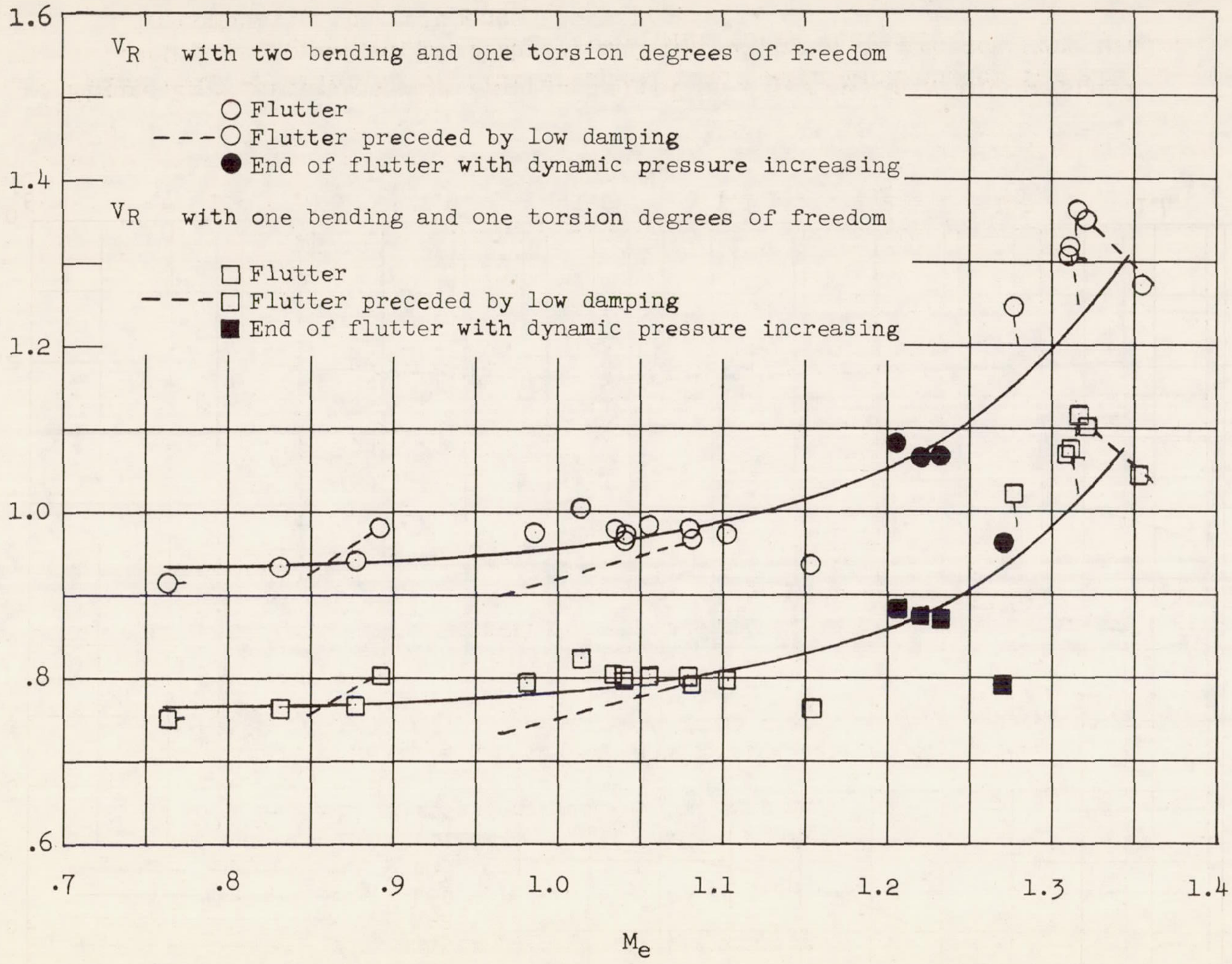

Figure 20.- Variation of flutter-speed ratio with Mach number for the 645 plan form when two and three degrees of freedom were used in computing the reference flutter speeds.

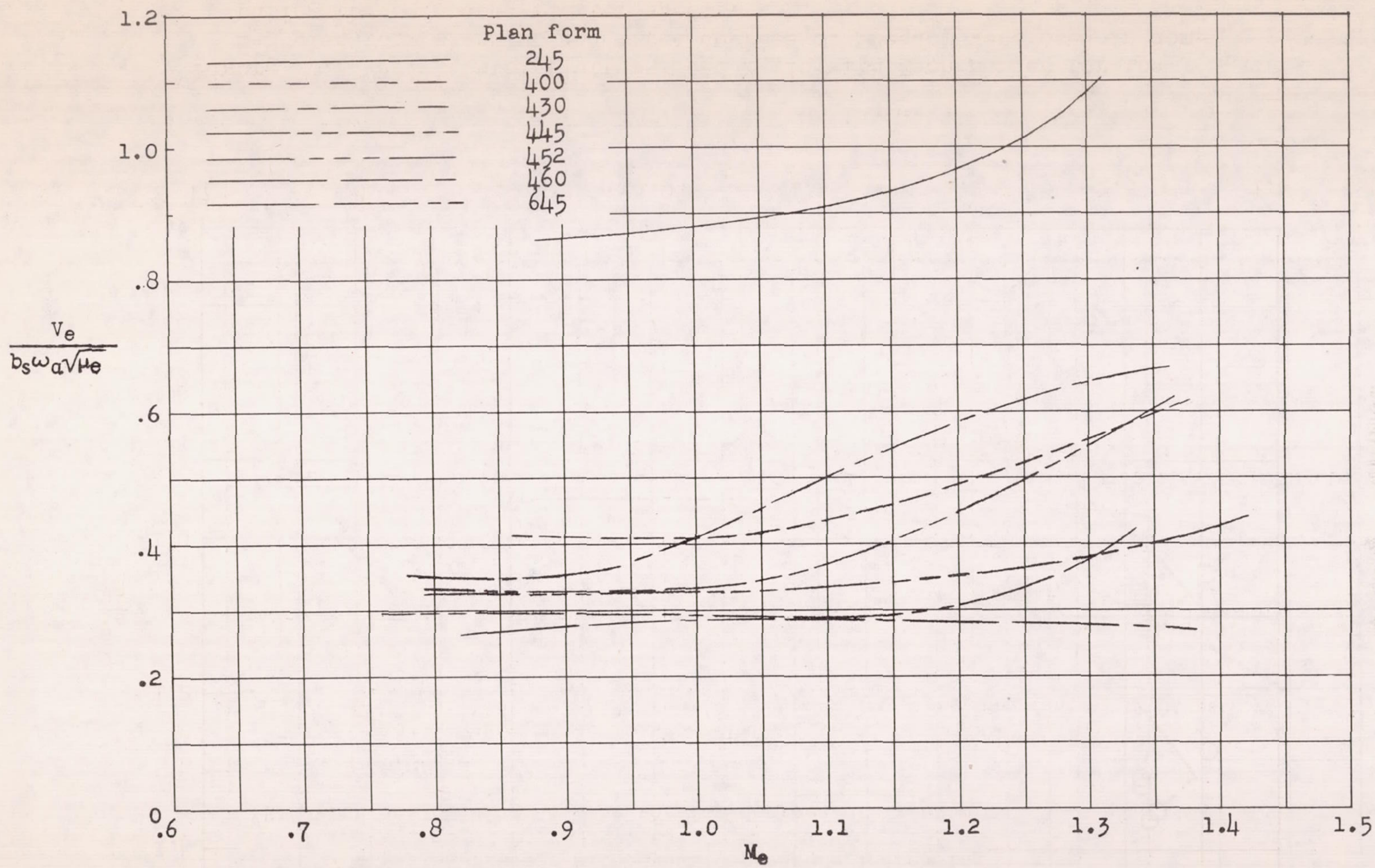

Figure 21.- Variation with Mach number of an experimental flutter-speed coefficient $\frac{V_e}{b_s \omega_\alpha \sqrt{\mu_e}}$ for plan forms tested.

CONFIDENTIAL

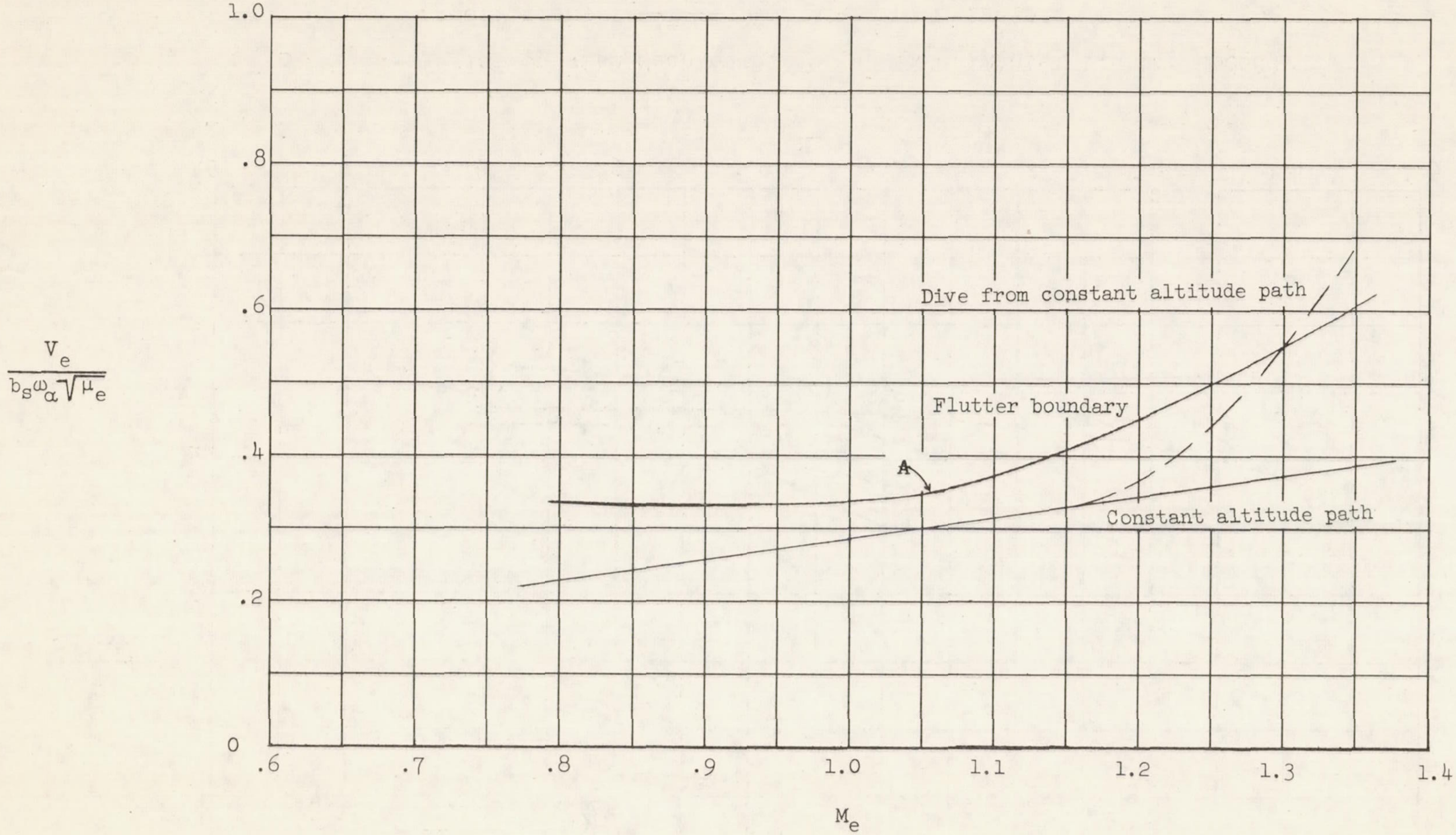

Figure 22.- Flutter boundary and hypothetical flight paths for 445 wing in terms of variation of $\frac{V_e}{b_s \omega_\alpha \sqrt{\mu_e}}$ with Mach number.

CONFIDENTIAL